Pergamon

*Int. J. Solids Structures* Vol. 35, No. 14, pp. 1589–1616, 1998
© 1998 Elsevier Science Ltd
All rights reserved. Printed in Great Britain
0020–7683/98 $19.00 + .00

PII: S0020–7683(97)00121–2

# ON THE CRITERION OF DAMAGE EVOLUTION FOR VARIABLE MULTIAXIAL STRESS STATES

A. SEWERYN
Bialystok University of Technology, Faculty of Mechanics, Wiejska 45 C, 15-351 Bialystok, Poland

Z. MRÓZ
Institute of Fundamental Technological Research, Polish Academy of Science, Świętokrzyska 21, 00-049 Warsaw, Poland

(*Received* 23 *July* 1996; *in revised form* 10 *April* 1997)

**Abstract**—The damage accumulation condition expressed in terms of traction components on a physical plane is discussed for both monotonic and cyclic loading conditions. The crack initiation is assumed to correspond to a critical value of damage reached on the physical plane. For singular stress distribution in the front of sharp notch or crack the non-local condition is formulated. The proposed condition is applied to predict damage distribution within the representative element for cyclic loading conditions. The rosette diagrams are constructed for visualization of damage distribution. The prediction of crack initiation for multiaxial fatigue loading is provided. The second- and fourth-order damage tensors in order to describe damage distribution within the element, and the associated compliance variation are introduced. © 1998 Elsevier Science Ltd.

## 1. INTRODUCTION

The present paper is concerned with the description of damage evolution for brittle materials such as rock, concrete, ceramics, some glassy polymers, and for metals under variable loading inducing fatigue crack initiation and propagation within the nominally elastic regime. The macroscopic plastic deformation can then be neglected and the inelastic strain is associated with the microcracking process. For high-cycle fatigue regime the microplastic effects occur at the level of dislocation interaction within crystalline lattice and the macroscopic response is usually treated as elastic with negligible effect of generating microcracks on the effective elastic moduli.

In the phenomenological models the damage is usually described by introducing scalar, vector or tensor state variables representing average crack density and orientation within the element. The specific elastic energy or free energy are then assumed as functions of strain tensor and of damage state variable, thus generating the framework for constitutive models providing the evolution rules of elastic compliance and damage. Starting from the early Kachanov work (1958) who introduced the scalar measure of damage, the subsequent investigators used different measures [cf Lemaitre (1992); Dragon and Mróz (1979); Krajcinovic (1989); Murakami (1988); Onat and Leckie (1988); Simo and Ju (1987); Chaboche (1992)]. A comparative study of description of crack density distribution in terms of scalar, second- and fourth-order tensors was provided by Lubarda and Krajcinovic (1993), following previous work by Onat and Leckie (1998) and Kanatani (1984). The specification of effective elastic moduli of damaged materials was considered by numerous authors [see, for instance, Budiansky and O'Connell (1976); Horii and Nemat-Nasser (1983); Lubarda and Krajcinovic (1994)].

In the present paper, we shall discuss the damage distribution within the representative element by assuming that the damage state is related to the history of contact tractions on a physical plane. The damage accumulated on a material facet can be represented by a scalar value associated with each facet. The macrocrack initiation is assumed to occur along the plane of critical damage value. For calculated distribution of damage, the respective tensor measure of crack density distribution can be specified. The elastic compliance

variation due to damage can be neglected when multiaxial fatigue problems are considered. However, this variation can be calculated by introducing interfacial strain components due to damage and averaging over all plane orientations within the element.

In Section 2 the conditions of brittle failure will be proposed for the case of monotonic loading. Both local and non-local conditions are considered, so the failure can be predicted for regular and singular stress regimes. Our analysis will follow the previous study of Seweryn and Mróz (1995), where the non-local stress condition was applied to study crack initiation and growth in brittle materials. The damage evolution for the case of multiaxial fatigue loading was analyzed by Seweryn and Mróz (1994, 1996).

In Section 3, the case of cyclic loading will be discussed and the previous analysis will be generalized. The case of combined cyclic bending and torsion will be discussed in Section 4 where the damage distribution and crack initiation will be predicted from the model. In Section 5, the second- and fourth-order damage tensors will be introduced in order to describe damage distribution within the element, and the associated compliance variation.

## 2. NON-LOCAL STRESS OR STRAIN CONDITION OF BRITTLE FAILURE

The crack initiation condition for non-singular stress concentrations in elastic bodies (near holes, rounded notches, etc.) is usually formulated in terms of local stresses. On the other hand, the existing crack propagation condition is usually expressed in terms of the critical value of the potential energy release due to crack growth (Griffith, 1920; Irwin, 1957; Palaniswamy and Knauss, 1972; Hussain *et al.*, 1974), critical value of crack opening displacement (Wells, 1961), or the critical value of strain energy at some distance from the crack tip [cf Sih (1974)]. However, for some singular stress concentrations, for instance generated by sharp edge shaped notches, the condition cannot be applied and the existence of crack emanating from the notch tip must be postulated.

### 2.1. *Stress condition*

In this section, we shall formulate the stress failure function which will specify the crack initiation in the representative element and also the damage accumulation on a physical plane. The stress condition will be expressed in terms of contact tractions acting on a selected plane and the crack initiation is assumed to occur on a plane of maximum value of the stress failure function.

A simple model is obtained by assuming that the stress value on any plane is associated with the tension and shear failure modes with the respective limit stress values $\sigma_c$ and $\tau_c$. The failure function will then specify the crack initiation condition for a combined stress action on a plane. To provide uniform treatment of crack initiation and propagation from stress concentrations, the non-local stress condition was proposed by Seweryn and Mróz (1995) and applied to predict both critical load value for crack initiation and also orientation of crack propagation. The experimental results obtained for notched specimens under combined tension and shear provided data confirming theoretical predictions of limit load values and crack orientations [cf Seweryn *et al.* (1997)]. The material response was assumed to be linear elastic and the generated crack length was specified by the assumed non-locality dimension.

This simple model was next extended to predict damage accumulation and fatigue crack initiation under multiaxial cyclic loading [cf Seweryn and Mróz (1994, 1996)]. It can be assumed that the failure function can be used in predicting damage on each physical plane by following the evolution of this function in the course of deformation process. The damage on any plane is assumed to be a scalar function $\omega_n$ affecting the values of failure stresses, thus $\sigma_c = \sigma_c(\omega_n)$, $\tau_c = \tau_c(\omega_n)$ on each plane. The distribution of $\omega_n$ will obviously depend on microcrack density distribution within the representative element. However, it is assumed, that strength and stiffness variation will depend on distribution of $\omega_n$, without explicit reference to crack density distribution.

The model development will follow the following steps:

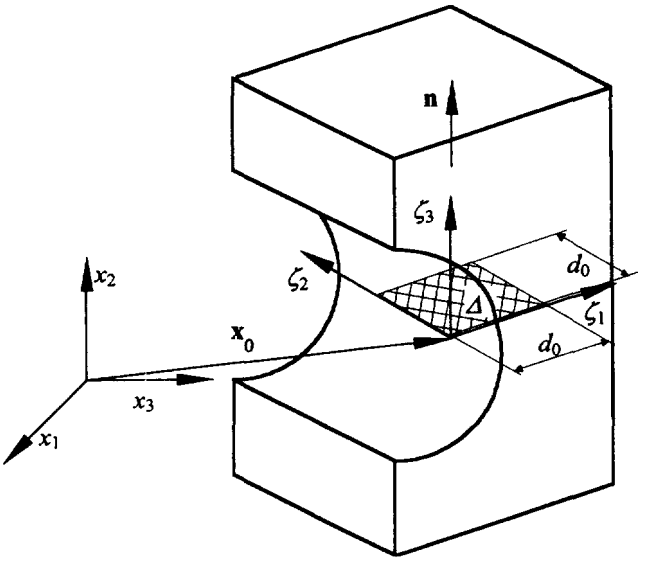


Fig. 1. Material plane element $\Delta$ at the notch surface.

(i) formulation of damage evolution $\omega_n(t)$ on each physical plane with account for monotonic or varying contact stress or strain histories;

(ii) specification of variation of $\sigma_c(\omega_n)$ and $\tau_c(\omega_n)$ and prediction of macrocrack initiation;

(iii) specification of elastic compliance or hardening variation due to distribution of $\omega_n$.

Let us note that for high-cycle fatigue problems the compliance variation is usually neglected and the crack initiation condition is specified through elastic stress history within the material element.

Consider a physical plane $\Delta$ and the local coordinate system $(\xi_1, \xi_2, \xi_3)$ (Fig. 1). The location of the material point in the facet with respect to the global reference system $(x_1, x_2, x_3)$ is specified by a position vector $\mathbf{x}_0(x_{01}, x_{02}, x_{03})$. The facet orientation is specified by a unit normal vector $\mathbf{n}(n_1, n_2, n_3)$, where $n_i = \cos(\xi_3, x_i)$. The traction vector $\mathbf{t} = \boldsymbol{\sigma}\mathbf{n}$ acting on the physical facet can be expressed in the local coordinate system by the relation

$$\Sigma_i(\tau_{n1}, \tau_{n2}, \sigma_n) = N_{ij}\sigma_{jk}n_k \tag{1}$$

where $\mathbf{N}$ is the orthogonal tensor of transformation, $N_{ij} = \cos(\xi_i, x_j)$. The shear stresses $\tau_{n1}$, $\tau_{n2}$ in the physical facet correspond to the coordinate axes $\xi_1$, $\xi_2$ and the resultant shear stress equals

$$\tau_n = [\tau_{n1}^2 + \tau_{n2}^2]^{1/2}. \tag{2}$$

The local stress condition of brittle failure is formulated by assuming that the crack initiation corresponds to critical value of the stress function $R_\sigma(\sigma_n, \tau_n)$ on any physical plane, thus

$$R_{f\sigma} = \max_{(\mathbf{n}, \mathbf{x}_0)} R_\sigma(\sigma_n/\sigma_c, \tau_n/\tau_c) = 1 \tag{3}$$

where $0 \leqslant R_{f\sigma} \leqslant 1$ is the brittle failure factor, $\sigma_c$ and $\tau_c$ denote the critical values of normal and shear stresses, $\mathbf{x}_0$ denotes the material point position and $\mathbf{n}$ is the physical facet orientation. The brittle failure function $R_\sigma(\sigma_n/\sigma_c, \tau_n/\tau_c)$ is expressed in terms of contact stress components $\sigma_n$, $\tau_n$ acting on the physical plane. Let us note that the condition (3) provides

crack location, orientation, and the critical load value. In fact, the location and orientation of crack is sought so that $R_\sigma$ is maximized with respect to $\mathbf{n}$ and $\mathbf{x}_0$.

The simplest example of the failure criterion is provided by considering only normal tensile stress $\sigma_n$, so that

$$R_\sigma(\sigma_n/\sigma_c) = \langle\sigma_n\rangle/\sigma_c \tag{4}$$

where $\langle\sigma_n\rangle = \sigma_n$ for $\sigma_n > 0$ and $\langle\sigma_n\rangle = 0$ for $\sigma_n < 0$. This condition corresponding to Mode I crack initiation is applicable for brittle materials for uniaxial or multiaxial stress states with tensile stress predominating. The other example of failure criterion is obtained by assuming the Mode II or III controlled by the shear stress, thus

$$R_\sigma(\tau_n/\tau_c) = |\tau_n|/\tau_c. \tag{5}$$

This condition can be applied for compressive stress regimes. It, however, does not account for the friction stress acting on the closed cracks interfaces. A more realistic criterion is obtained by applying the Coulomb condition

$$R_\sigma(\sigma_n/\sigma_c, \tau_n/\tau_c) = \frac{1}{\tau_c}(|\tau_n| + \sigma_n \tan\varphi) \tag{6}$$

combined with the normal stress condition (4). Here, $\varphi$ denotes the friction angle on the crack interface.

In the previous study [cf Seweryn and Mróz (1994, 1995)], the elliptic condition combined with the shear condition was applied, thus

$$R_\sigma\left(\frac{\sigma_n}{\sigma_c}, \frac{\tau_n}{\tau_c}\right) = \left[\left(\frac{\langle\sigma_n\rangle}{\sigma_c}\right)^2 + \left(\frac{\tau_n}{\tau_c}\right)^2\right]^{0.5}. \tag{7}$$

Figure 2 presents these failure conditions in the $(\sigma_n, \tau_n)$-plane. The critical failure planes

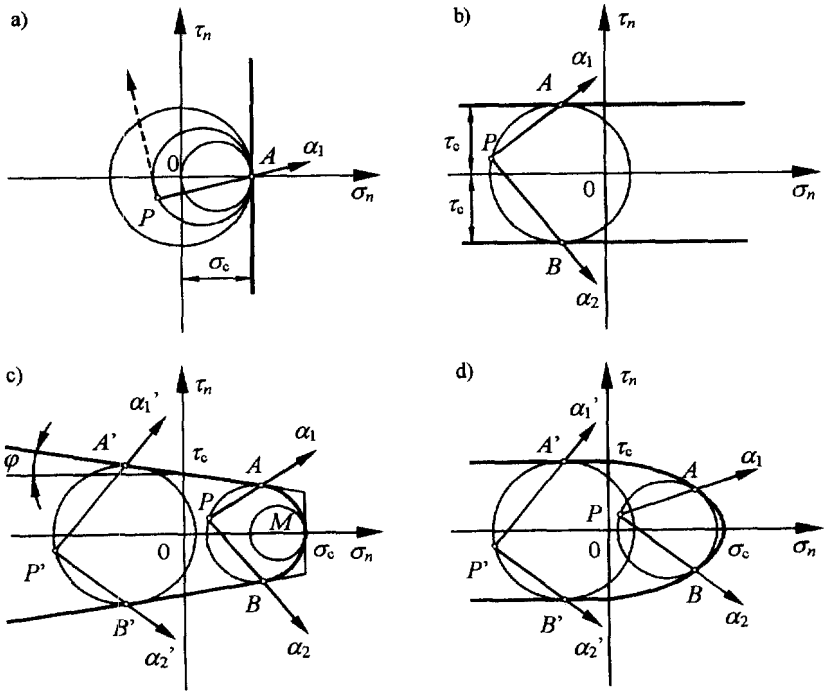


Fig. 2. Failure stress functions: (a) tension condition; (b) shear condition; (c) Coulomb condition with tension cut-off; (d) elliptic condition in tensile regime combined with shear condition in compressive regime.

are then specified by means of Mohr circles, tangent to the respective failure lines. Generally, two critical planes $\alpha_1$ and $\alpha_2$ are obtained, except for the normal stress condition (4).

For singular or quasi-singular stress distributions with very large stress gradients, the mean stress $\bar{\sigma}_n$ and $\bar{\tau}_n$ over the area $d_0 \times d_0$ on the critical plane are specified [cf Novozhilov (1969); Seweryn (1994); Seweryn and Mróz (1995)], so that

$$\bar{\sigma}_n = \frac{1}{d_0^2}\int_0^{d_0}\int_0^{d_0} \sigma_n \, d\xi_1 \, d\xi_2, \quad \bar{\tau}_n = \frac{1}{d_0^2}\int_0^{d_0}\int_0^{d_0} \tau_n \, d\xi_1 \, d\xi_2. \tag{8}$$

The non-local failure condition is now specified as follows

$$R_{f\sigma} = \max_{(\mathbf{n},\mathbf{x}_0)} \bar{R}_\sigma(\bar{\sigma}_n/\sigma_c, \bar{\tau}_n/\tau_c) = 1. \tag{9}$$

Alternatively, the failure function is averaged over the area $d_0 \times d_0$, thus

$$R_{f\sigma} = \max_{(\mathbf{n},\mathbf{x}_0)} \bar{R}_\sigma(\sigma_n/\sigma_c, \tau_n/\tau_c) = \max_{(\mathbf{n},\mathbf{x}_0)} \left[\frac{1}{d_0^2}\int_0^{d_0}\int_0^{d_0} R_\sigma \, d\xi_1 \, d\xi_2\right] = 1. \tag{10}$$

The non-local criteria (9) and (10) are equivalent when $R_\sigma$ is a linear function of contact stress components. The value of $d_0$ can now be related to microstructural parameters, for instance, grain size. To make the non-local model equivalent to Griffith–Irwin crack propagation condition $K_I = K_{Ic}$ in Mode I, the value of $d_0$ can be identified [cf Seweryn (1994)], thus

$$d_0 = \frac{2}{\pi}\left(\frac{K_{Ic}}{\sigma_c}\right)^2 \tag{11}$$

where $K_{Ic}$ is the critical value of the stress intensity factor.

Let us now introduce the microplastic damage variable $0 \leqslant \omega_{n\sigma} \leqslant 1$ on a physical plane $\Delta$. This variable is assumed to affect the failure stress values, thus

$$\begin{aligned} \sigma_c &= \sigma_c(T, \omega_{n\sigma}) = \sigma_{c0}(T)(1-\omega_{n\sigma})^p \\ \tau_c &= \tau_c(T, \omega_{n\sigma}) = \tau_{c0}(t)(1-\omega_{n\sigma})^p \end{aligned} \tag{12}$$

where $\sigma_{c0}$ and $\tau_{c0}$ are temperature dependent failure stresses for the undamaged material and $\omega_{n\sigma}$ is a scalar measure of brittle damage on the plane. Equation (12) implies the relations

$$\omega_{n\sigma} = 1 - \left(\frac{\sigma_c}{\sigma_{c0}}\right)^{1/p} = 1 - \left(\frac{\tau_c}{\tau_{c0}}\right)^{1/p} \tag{13}$$

where $p$ denotes material parameter. Let us note that for $p \ll 1$, there will be very insignificant variation of $\sigma_c$ and $\tau_c$ for stress states not approaching the actual failure surface. The relations (12) must be accompanied by the evolution rule for $\omega_{n\sigma}$. The specific form of the damage evolution rule will be discussed in detail in Section 3 for the case of high-cycle fatigue loading.

A more general assumption can now be introduced, when accounting for damage due to macroplastic deformation, creep and corrosive effect. Denoting the respective damage values by $\omega_{np}$, $\omega_{nv}$, $\omega_{nh}$, the global damage measure $\omega_n$ can be introduced, so that

$$\omega_n = \omega_{n\sigma} + \Phi_\sigma(\omega_{np}, \omega_{nv}, \omega_{nh}) \tag{14}$$

and

$$\sigma_c = \sigma_{c0}(T)(1-\omega_n)^p \quad \tau_c = \tau_{c0}(T)(1-\omega_n)^p \tag{15}$$

where $\Phi_\sigma(\omega_{np}, \omega_{nv}, \omega_{nh})$ is the damage measure due to dissipative process. In this paper, the specification of $\Phi_\sigma(\omega_{np}, \omega_{nv}, \omega_{nh})$ will not be discussed.

2.2. *Strain condition*

An alternative condition of failure can be expressed in terms of contact strain components $\gamma_{n1}$, $\gamma_{n2}$, $\varepsilon_n$ on the plane $\Delta$, where $\varepsilon_n$ denotes the normal strain and $\gamma_{n1}$, $\gamma_{n2}$ are the shear strains in the local coordinate system $(\xi_1, \xi_2, \xi_3)$, thus

$$E_i(\gamma_{n1}, \gamma_{n2}, \varepsilon_n) = N_{ij}\varepsilon_{jk}n_k. \tag{16}$$

The resultant shear strain equals

$$\gamma_n = [\gamma_{n1}^2 + \gamma_{n2}^2]^{1/2}. \tag{17}$$

The local failure condition can be expressed in terms of the contact strain components, namely

$$R_{f\varepsilon} = \max_{(\mathbf{n},\mathbf{x}_0)} R_\varepsilon(\varepsilon_n/\varepsilon_c, \gamma_n/\gamma_c) = 1 \tag{18}$$

where $\varepsilon_c$, $\gamma_c$ are the critical failure strain values, and $R_\varepsilon(\varepsilon_n, \gamma_n)$ denotes the strain failure function. Similar to eqn (7), we can now postulate

$$R_\varepsilon\left(\frac{\varepsilon_n}{\varepsilon_c}, \frac{\gamma_n}{\gamma_c}\right) = \left[\left(\frac{\langle\varepsilon_n\rangle}{\varepsilon_c}\right)^2 + \left(\frac{\gamma_n}{\gamma_c}\right)^2\right]^{0.5}. \tag{19}$$

The non-local strain failure condition can be written analogously to eqns (9) or (10), thus

$$R_{f\varepsilon} = \max_{(\mathbf{n},\mathbf{x}_0)} \bar{R}_\varepsilon(\varepsilon_n/\varepsilon_c, \gamma_n/\gamma_c) = \max_{(\mathbf{n},\mathbf{x}_0)} \left[\frac{1}{d_\varepsilon^2}\int_0^{d_\varepsilon}\int_0^{d_\varepsilon} R_\varepsilon \, d\xi_1 \, d\xi_2\right] = 1. \tag{20}$$

It should be noted that the stress and strain conditions are not equivalent, since $\varepsilon_n$ depends on $\sigma_n$ and $\sigma_{t1}$, $\sigma_{t2}$ acting within the contact plane, and $\sigma_n$ depends on strain components $\varepsilon_n$ and $\varepsilon_{t1}$, $\varepsilon_{t2}$. Figure 3(a, b) presents the condition (7) in the strain plane $(\varepsilon_n, \gamma_n)$ for the plane stress case assuming $\tau_c/\sigma_c = \sqrt{3}$ and $1/\sqrt{3}$, $\nu = 0.3$. It is seen that the ratio $\varepsilon_t/\varepsilon_n$ of the tangential and normal strain effects the condition.

## 3. DAMAGE DISTRIBUTION DUE TO MULTIAXIAL FATIGUE LOADING

In this section we shall develop the damage evolution rule in the case of multiaxial fatigue loading within the elastic domain, so the macroplastic strains do not occur in the steady cyclic state. The growth of microplastic (or brittle) damage on a physical plane is assumed to depend on the contact stress, damage state, and stress increment, thus

$$d\omega_{n\sigma} = d\omega_{n\sigma}(\boldsymbol{\Sigma}, d\boldsymbol{\Sigma}, \omega_n). \tag{21}$$

In the stress plane the domain of no damage accumulation is specified by the inequality

a)

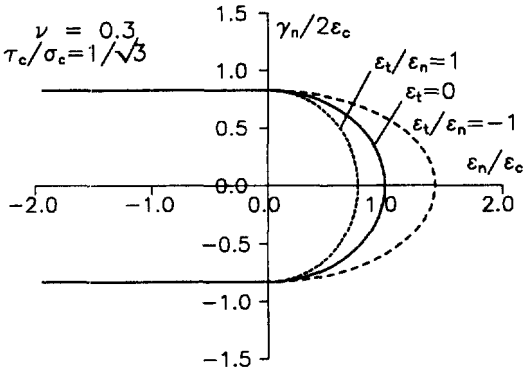


b)

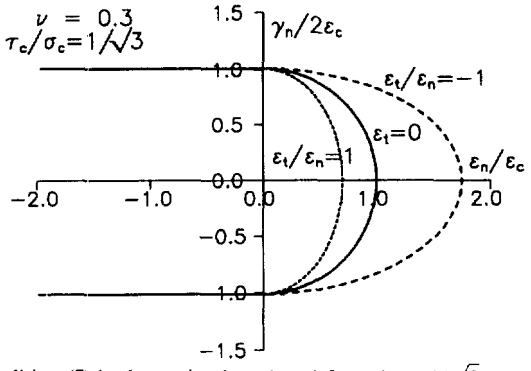


Fig. 3. The stress condition (7) in the strain plane $(\varepsilon_n, \gamma_n)$ for $\sigma_c/\tau_c = 1/\sqrt{3}$, $\nu = 0.3$: (a) plane stress; (b) plane strain.

$$R_{\sigma 0}\left(\frac{\sigma_n}{\sigma_0}, \frac{\tau_n}{\tau_0}\right) \leqslant 1 \tag{22}$$

and the damage initiation locus corresponds to the value $R_{f\sigma 0} = R_{\sigma 0} = 1$. The damage accumulation thus occurs in the exterior of the domain $R_{\sigma 0} \leqslant 1$ and the scalar value $R_{f\sigma 0}$ is calculated on the physical plane

$$R_{f\sigma 0} = \max_{(\mathbf{n}, \mathbf{x}_0)} R_{\sigma 0}\left(\frac{\sigma_n}{\sigma_0}, \frac{\tau_n}{\tau_0}\right) > 1 \tag{23}$$

where $\sigma_0$, $\tau_0$ are the damage initiation stresses in tension and shear.

For large values of the stress gradient, the non-local condition is expressed in terms of mean stress values over the area $d_0 \times d_0$, thus

$$\bar{R}_{f\sigma 0} = \max_{(\mathbf{n}, \mathbf{x}_0)} \bar{R}_{\sigma 0}\left(\frac{\bar{\sigma}_n}{\sigma_0}, \frac{\bar{\tau}_n}{\tau_0}\right) > 1 \tag{24}$$

or in terms of the averaged value of $R_{\sigma 0}$, so that

$$\bar{R}_{f\sigma 0} = \max_{(\mathbf{n},\mathbf{x}_0)} \bar{R}_{\sigma 0}\left(\frac{\sigma_n}{\sigma_0}, \frac{\tau_n}{\tau_0}\right) = \max_{(\mathbf{n},\mathbf{x}_0)} \left[\frac{1}{d_0^2}\int_0^{d_0}\int_0^{d_0} R_{\sigma 0}\left(\frac{\sigma_n}{\sigma_0}, \frac{\tau_n}{\tau_0}\right) d\xi_1\, d\xi_2\right] = 1. \tag{25}$$

The damage initiation stress $\sigma_0$, $\tau_0$ may in general depend on temperature and the damage previously accumulated, so we have

$$\begin{aligned} \sigma_0 &= \sigma_0(T, \omega_n) = \sigma_{00}(T)(1-\omega_n)^{p^*} \\ \tau_0 &= \tau_0(T, \omega_n) = \tau_{00}(T)(1-\omega_n)^{p^*} \end{aligned} \tag{26}$$

where $p^*$ is material parameter.

Consider the domain $\Omega_d$ bounded by damage initiation and stress failure curves (Fig. 4). Assume, for simplicity, that $\sigma_0(\omega_n) = f\sigma_c(\omega_n)$, $\tau_0(\omega_n) = f\tau_c(\omega_n)$. Consider a family of curves

$$R_\sigma\left(\frac{\sigma_n}{\sigma_c}, \frac{\tau_n}{\tau_c}\right) = \left[\left(\frac{\langle\sigma_n\rangle}{\sigma_c}\right)^2 + \left(\frac{\tau_n}{\tau_c}\right)^2\right]^{0.5} = c = \text{const.} \tag{27}$$

For $R_\sigma = 1$, the curve coincides with the stress failure locus, for $R_\sigma = f$ with the damage initiation locus, $R_{\sigma 0} = 1$. The damage growth can be specified by the following relation

$$d\omega_{n\sigma} = \Psi_\sigma(R_\sigma)\, d\hat{R}_\sigma \tag{28}$$

where

$$d\hat{R}_\sigma = \begin{cases} dR_\sigma & \text{for } dR_\sigma > 0 \text{ and } R_\sigma > f \\ 0 & \text{for } dR_\sigma \leqslant 0 \text{ or } R_\sigma \leqslant f \end{cases} \tag{29}$$

and

$$dR_\sigma = \frac{\partial R_\sigma}{\partial(\sigma_n/\sigma_c)} d\left(\frac{\sigma_n}{\sigma_c}\right) + \frac{\partial R_\sigma}{\partial(\tau_n/\tau_c)} d\left(\frac{\tau_n}{\tau_c}\right) = \frac{\partial R_\sigma}{\partial \sigma_n} d\sigma_n + \frac{\partial R_\sigma}{\partial \tau_n} d\tau_n + \frac{\partial R_\sigma}{\partial \omega_n} d\omega_n. \tag{30}$$

Let us note that the damage growth occurs for all loading events satisfying eqn (29). Thus, the loading surface $R_\sigma = c$ in the cyclic loading process expands and shrinks, and the stress point always remains on the surface. For instance, when the stress path is straight with the stress point oscillating between zero and maximal value, the damage accumulation will occur on each stress path portion, corresponding to loading event.

Neglecting the effect of damage accumulation on $R_\sigma$, and assuming the damage condition (7), we have

$$dR_\sigma = \frac{1}{R_\sigma}\left(\frac{\langle\sigma_n\rangle\, d\sigma_n}{\sigma_c^2} + \frac{\tau_n\, d\tau_n}{\tau_c^2}\right). \tag{31}$$

The damage accumulation thus occurs for stress paths directed into the exterior of the domain bounded by the curve $R_\sigma = \text{const}$ from the actual stress point $P$ [Fig. 4(a)].

An alternative specification of loading–unloading domains was presented by Seweryn and Mróz (1994), Fig. 4(b). Introducing two planes moving with the stress point

$$\begin{aligned} \phi_1 &= \hat{\sigma}_n - \sigma_n^+(t) \leqslant 0 \\ \phi_2 &= \hat{\tau}_{ni}^2 - \tau_{ni}^2(t) \leqslant 0 \end{aligned} \tag{32}$$

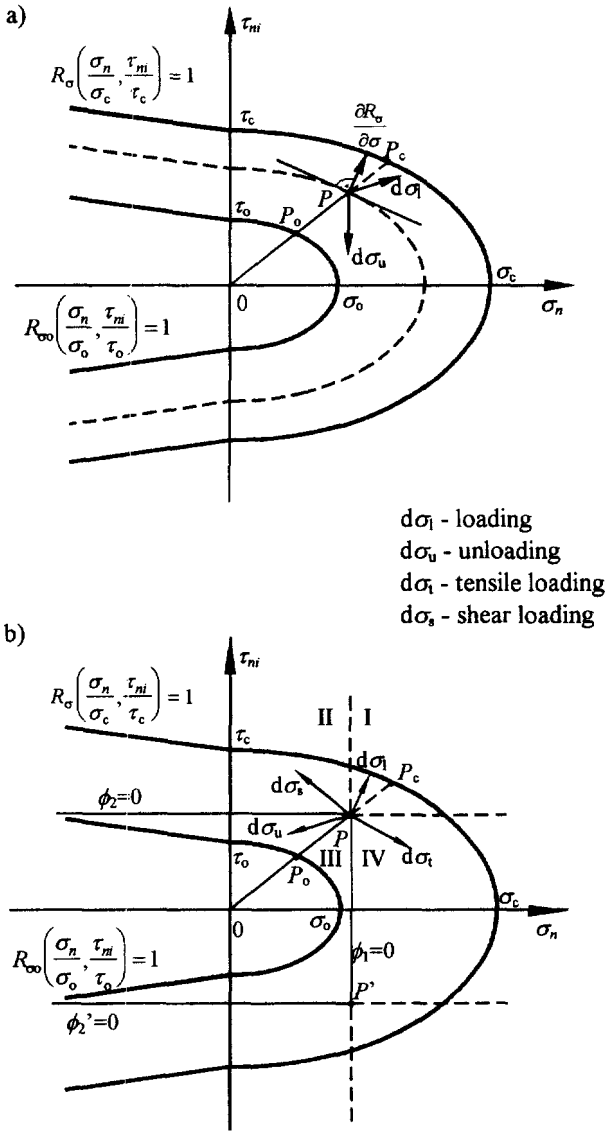


Fig. 4. Damage initiation and stress failure curves in the $(\sigma_n, \tau_n)$-plane: (a) loading–unloading domains specified by the curves $R_\sigma = \text{const}$; (b) loading–unloading domains specified by straight lines $\phi_1 = 0$, $\phi_2 = 0$.

where $\sigma_n^+(t)$ and $\tau_{ni}(t)$ are the actual values of tensile stress and shear stress, the damage accumulation is assumed to occur when

$$\begin{aligned} &\phi_1 = 0, \quad d\phi_1 > 0 \quad \text{or } \hat{\sigma}_n = \sigma_n^+(t), \quad d\sigma_n > 0 \\ &\phi_2 = 0, \quad d\phi_2 > 0 \quad \text{or } \hat{\tau}_{ni}^2 = \tau_{ni}^2(t), \quad \tau_{ni}\, d\tau_{ni} > 0. \end{aligned} \tag{33}$$

We have then

$$d\hat{R}_\sigma = \frac{\partial R_\sigma}{\partial \sigma_n} d\hat{\sigma}_n + \frac{\partial R_\sigma}{\partial \tau_{n1}} d\hat{\tau}_{n1} + \frac{\partial R_\sigma}{\partial \tau_{n2}} d\hat{\tau}_{n2} + \frac{\partial R_\sigma}{\partial \omega_n} d\omega_n \tag{34}$$

where effective stress increments (for $R_{\sigma 0} > 1$) are specified by the following relations

$$d\hat{\sigma}_n = d\sigma_n \quad \text{for } d\sigma_n \geqslant 0 \quad \text{and} \quad \sigma_n \geqslant 0$$
$$d\hat{\sigma}_n = 0 \quad \text{for } d\sigma_n < 0 \quad \text{or} \quad \sigma_n < 0 \tag{35a}$$

and

$$d\hat{\tau}_{ni} = d\tau_{ni} \quad \text{for } \tau_{ni}\, d\tau_{ni} \geqslant 0$$
$$d\hat{\tau}_{ni} = 0 \quad \text{for } \tau_{ni}\, d\tau_{ni} < 0. \tag{35b}$$

The conditions (35) specify three loading and one unloading quadrantal domains: I, corresponding to full loading, II, corresponding to shear loading, III, corresponding to unloading, and IV corresponding to tension loading [Fig. 4(b)].

The non-local measure of the increment of damage function is specified as follows

$$d\bar{\hat{R}}_\sigma = \frac{1}{d_0^2}\int_0^{d_0}\int_0^{d_0} d\hat{R}_\sigma\, d\xi_1\, d\xi_2. \tag{36}$$

More complex damage evolution rules can be formulated by following the multisurface plasticity hardening rules [cf Mróz (1983)] and introducing the set of nested surfaces memorizing particular loading events.

The damage function can be assumed in the following form [cf Seweryn and Mróz (1994)]

$$\Psi_\sigma(R_\sigma) = A_\sigma \left(\frac{\langle R_\sigma - R_{\sigma 0c}\rangle}{1 - R_{\sigma 0c}}\right)^{n_\sigma} \frac{1}{1 - R_{\sigma 0c}} \tag{37}$$

where $n_\sigma$ and $A_\sigma$ are the material parameters and $R_{\sigma 0c} = R_\sigma / R_{\sigma 0}$. Referring to Fig. 5, the geometric interpretation can be described in eqn (33) by taking $PP_0 = R_\sigma - R_{\sigma 0c}$, $P_cP_0 = 1 - R_{\sigma 0c}$, $P_cP = 1 - R_\sigma$.

Consider now the uniaxial tension test with $\sigma$ varying in the damage accumulation domain. Assuming the damage accumulation rule (28) and the damage function specified by eqn (37), we obtain

$$d\omega_{n\sigma} = A_\sigma \frac{\langle \sigma - \sigma_0 \rangle^{n_\sigma}}{(\sigma_c - \sigma_0)^{n_\sigma + 1}} d\sigma \tag{38}$$

where $\sigma_0$ is the fatigue endurance stress. The critical physical plane is now normal to the tension axis, and there is no damage accumulation for $\sigma < \sigma_0$. Accounting for coupling between damage and the failure stress, eqn (12), we assume

$$\sigma_c = \sigma_{c0}(T)(1 - \omega_{n\sigma}) \quad \tau_c = \tau_{c0}(T)(1 - \omega_{n\sigma}). \tag{39}$$

Assuming $\sigma_0 = 0$ and integrating eqn (38) we obtain

$$\int_0^{\omega_1} (1 - \omega_{n\sigma})^{n_\sigma + 1}\, d\omega_{n\sigma} = \frac{A_\sigma}{\sigma_{c0}^{n_\sigma + 1}} \int_0^{\sigma_{c1}} \sigma^{n_\sigma}\, d\sigma \tag{40}$$

where $\sigma_{c1}$ is the tensile failure stress. Equation (40) provides the relation

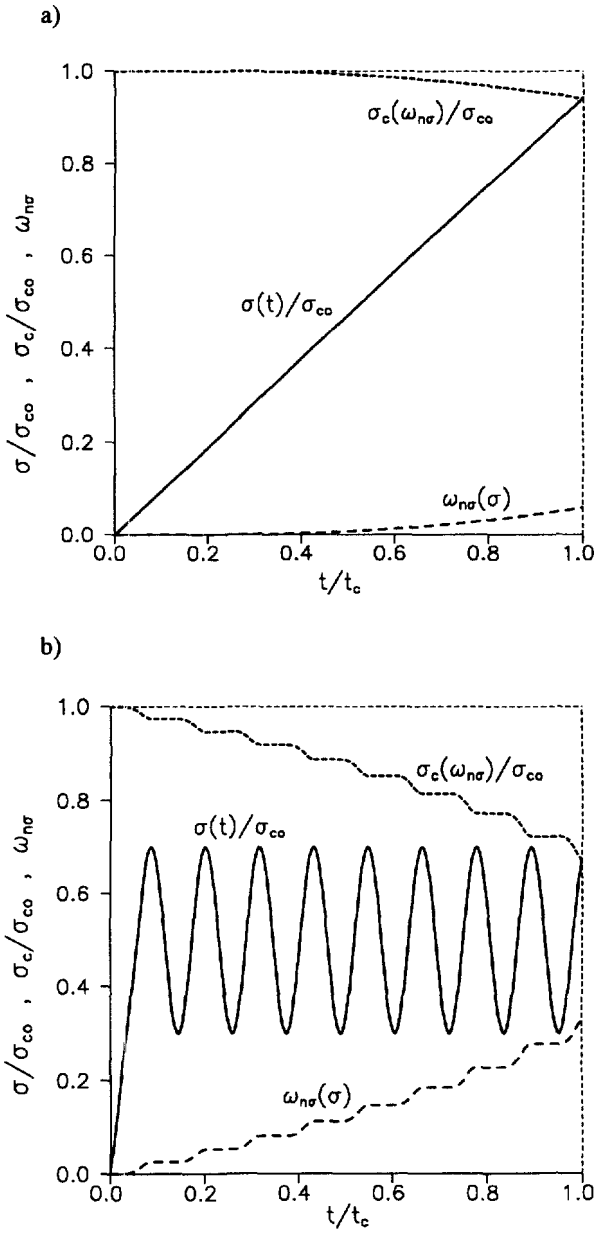


Fig. 5. Evolution of damage $\omega_{n\sigma}(\sigma)$ and of critical stress $\sigma_c(\omega_{n\sigma})$ for (a) monotonic; and (b) cyclic loading.

$$(1-\omega_1)^{n_\sigma+1}\left(1-\omega_1+A_\sigma\frac{n_\sigma+2}{n_\sigma+1}\right)=1 \tag{41}$$

specifying the damage value $\omega_1$. The variation of $\sigma_c$ is then specified by eqn (39).

Figure 5 presents the evolution of $\sigma_c(\omega_{n\sigma})$ in the course of monotonic and cyclic loading. In Fig. 5(a), the monotonic loading process is presented. For increasing stress $\sigma(t)$ the damage accumulation $\omega_{n\sigma}$ on the critical plane increases and the failure stress $\sigma_c(\omega_{n\sigma})$ decreases. When $\sigma(t) = \sigma_c(\omega_{n\sigma})$, the brittle failure occurs. Figure 5(b) presents the process of damage accumulation for high cycle fatigue loading. For specified stress amplitude and mean stress values, the damage accumulation induces the decrease of failure stress $\sigma_c(\omega_{n\sigma})$. When the maximal stress reaches the value of failure stress, the crack initiation occurs in the element.

In the case of high cycle fatigue, an alternative formulation can be proposed by neglecting variation of $\sigma_c$ and $\tau_c$ and assuming $R_\sigma = R_\sigma(\sigma_n, \tau_n)$. However, the damage evolution rule is modified, namely

$$\omega_{n\sigma} = \int_0^{\hat{R}_\sigma} A_1 \Psi_\sigma(R_\sigma)\, \mathrm{d}\hat{R}_\sigma \tag{42}$$

where $\mathrm{d}\hat{R}_\sigma$ is specified by eqn (28) or (31) and $A_1$ is material parameter. This type of evolution rule was considered by Seweryn and Mróz (1994, 1996). The crack initiation occurs on the physical plane where the damage measure $R_d$ reaches its critical value

$$R_d = \max_{(\mathbf{n},\mathbf{x}_0)} \omega_{n\sigma} = 1. \tag{43}$$

For singular or quasi singular stress distribution, the non-local condition presented by eqn (9) or (10) is used. The crack length growth is specified by the rule

$$\mathrm{d}a = \max_{(\mathbf{n},\mathbf{x}_0)} [A_2 \Psi_\sigma(\bar{R}_\sigma)\, \mathrm{d}\bar{\hat{R}}_\sigma] \tag{44}$$

where $A_2$ is the material parameter. The vector $\mathbf{x}_0$ corresponds to the crack tip and the vector $\mathbf{n}$ provides the propagation direction associated with the maximum of eqn (44).

## 4. DAMAGE ACCUMULATION IN ELEMENTS UNDER COMBINED FLEXURAL AND TORSIONAL CYCLIC LOADING

In this section, the damage accumulation condition (42) will be applied to study damage distribution and crack initiation for the case of cyclic loading of a cylinder by the combined bending and torsion. Assume that

$$\frac{\sigma_0}{\sigma_c} = \frac{\tau_0}{\tau_c} = f \tag{45}$$

so that damage and crack initiation conditions $R_{\sigma 0} = 1$ and $R_\sigma = 1$ are specified by similar relations. Referring to Fig. 4, introduce in the stress plane $(\sigma_n, \tau_n)$ a set of one-parameter curves $R_\sigma = \text{const}$, $(f \leqslant R_\sigma \leqslant 1)$ specified by the condition (7). Assuming the accumulation function (37), the crack initiation condition (43) takes the form

$$R_d = \max_{(\mathbf{n},\mathbf{x}_0)} \left[ \int_0^{\hat{R}_d} A_1 \left( \frac{R_\sigma - f}{1-f} \right)^{n_\sigma} \frac{\mathrm{d}\hat{R}_\sigma}{1-f} \right] = 1. \tag{46}$$

Geometrically, for any stress point $P$ within the domain $\Omega_d$, the radial distance of this point from the curve $R_{\sigma 0} = 1$ equals $PP_0$ and the radial distance between the curves $R_\sigma = 1$ and $R_{\sigma 0} = 1$ equals $P_0P_c$. We have then

$$\left( \frac{R_\sigma - f}{1-f} \right)^{n_\sigma} = \left( \frac{PP_0}{P_cP_0} \right)^{n_\sigma}. \tag{47}$$

Consider a cylindrical element under cyclic loading by the bending and torsional moments

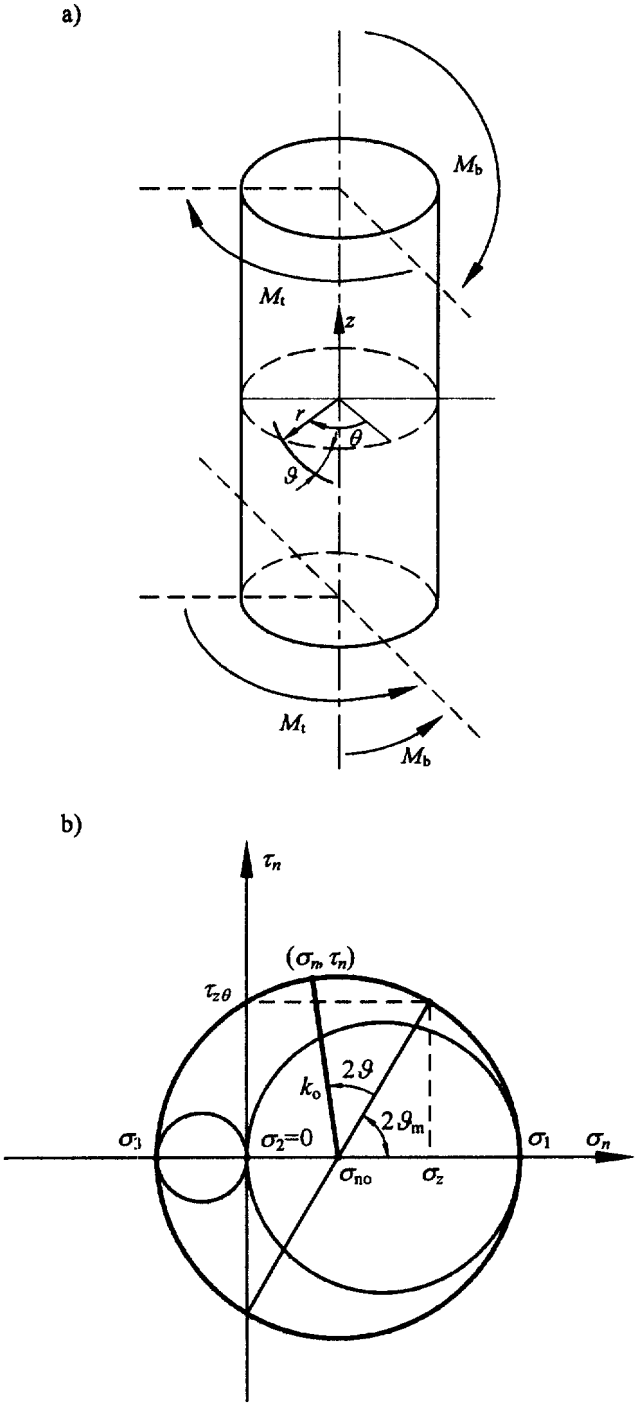


Fig. 6. (a) Cylinder subjected to combined bending and torsion; (b) Mohr circle.

[Fig. 6(a)]. The resulting stress components are the axial stress $\sigma_z$ and the shear stress $\tau_{r\theta}$ within the cross-section normal to the element axis. The maximal values of stresses occur at the cylindrical surface and can be presented as follows:

$$\sigma_z(t) = \sigma_a \sin(\omega_t t) + \sigma_m$$
$$\tau_{z\theta}(t) = \tau_a \sin(\omega_t t - \delta) + \tau_m \tag{48}$$

where $\sigma_a$, $\tau_a$ are the normal and shear stress amplitudes, $\sigma_m$, $\tau_m$ denote their mean values and $\delta$ is the phase angle of two stress components. The cylindrical surface is traction-free,

hence $\sigma_{rr} = \tau_{r\theta} = \tau_{rz} = 0$. Further, it is assumed that the circumferential stress $\sigma_{\theta\theta}$ vanishes. Using the stress circle, Fig. 6(b), the stress components acting on any plane normal to the cylindrical surface are

$$\sigma_n = \sigma_{n0} + k_0 \cos 2(\vartheta + \vartheta_m)$$
$$\tau_n = k_0 \sin 2(\vartheta + \vartheta_m) \tag{49}$$

where

$$\sigma_{n0} = \sigma_z/2, \quad k_0^2 = \left(\frac{\sigma_z}{2}\right)^2 + \tau_{z\theta}^2$$

and $\vartheta$ denotes the angle of orientation of the plane with respect to circumferential direction, and $\vartheta_m$ denotes the orientation of the major principal stress plane.

The crack initiation condition for in-plane ($\delta = 0$) fatigue loading was studied by Seweryn and Mróz (1996) in the related paper. In this section, we shall present the fatigue damage distribution $\omega_{n\sigma}$ and the maximal damage $R_d$ within the surface element for one cycle of out-of-phase loading ($\delta \neq 0$). The amplitude of loading was assumed at a level corresponding to a specified value of $R_{f\sigma}$ for proportional loading in one semicycle. The effect of phase angle $\delta$ is studied in detail for a brittle material for which $\sigma_c/\tau_c = 1/\sqrt{3}$ and for a steel for which $\sigma_c/\tau_c = \sqrt{3}$.

Figure 7(a, b) presents the damage accumulation on the extremal plane for the evolution rule given by eqns (28) and (35) during one cycle of in-phase loading ($\delta = 0$) and for the stress amplitude corresponding to $R_{f\sigma} = 0.5$. It is assumed that $n_\sigma = 1$, $f = 0.2$ and bending loading only, $\tau_m = \tau_a = 0$, $\sigma_m = 0$. Figure 7(a) corresponds to $\sigma_c/\tau_c = 1/\sqrt{3}$ and Fig. 7(b) to $\sigma_c/\tau_c = \sqrt{3}$. The portions of stress cycle for which damage accumulation occurs are marked as thickened segments. The first diagram presents the variation of $\sigma_z$ and $\tau_{z\theta}$, the second diagram presents the variation of $\sigma_n$ and $\tau_n$ on the extremal plane, third diagram provides the variation of the brittle failure function $R_\sigma$ on the extremal plane and the last

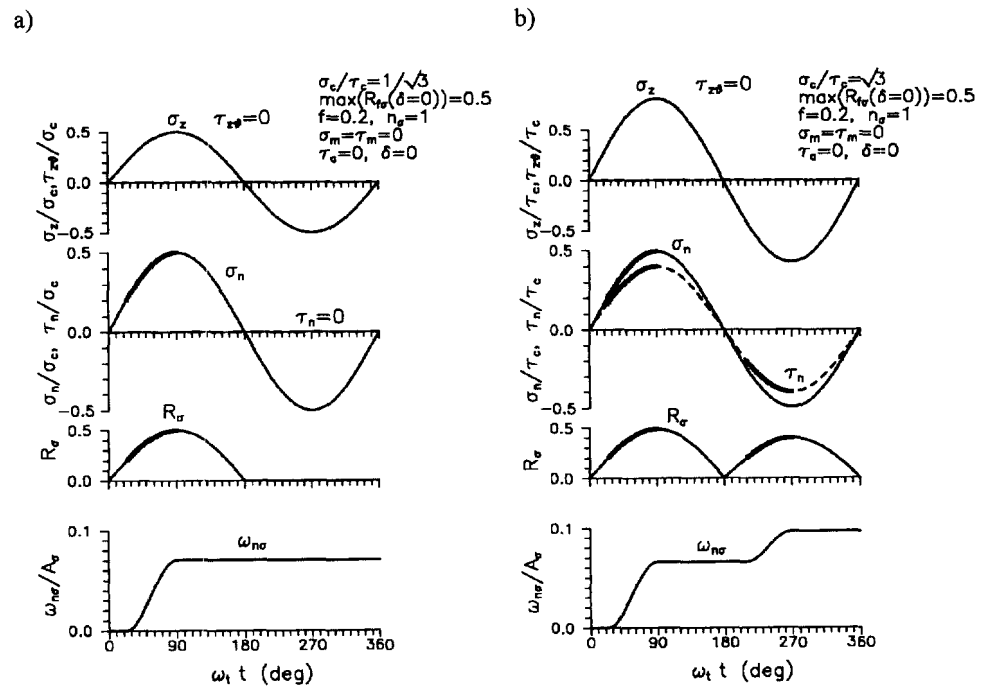


Fig. 7. Damage accumulation on the extremal plane for bending one loading cycle; $\max(R_{f\sigma}) = 0.5$, $f = 0.2$, $n_\sigma = 1$, $\tau_a = \tau_m = \sigma_m = 0$, $\delta = 0$. The ratio $\sigma_c/\tau_c$ equals: (a) $1/\sqrt{3}$; (b) $\sqrt{3}$.

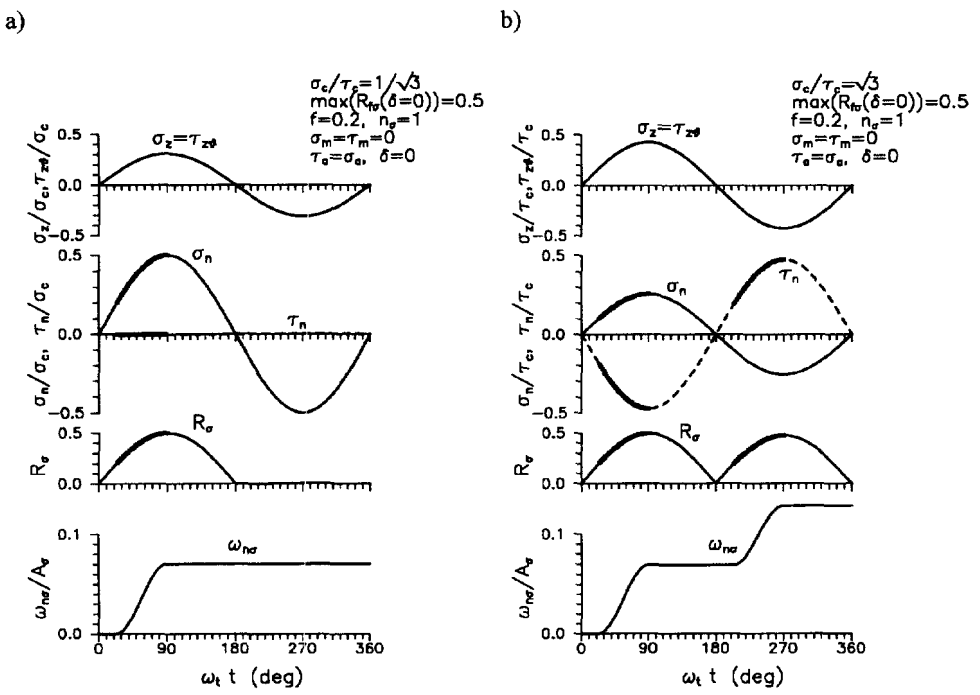


Fig. 8. Damage accumulation on the extremal plane during proportional bending and torsional one loading cycle for $\max(R_{f\sigma}) = 0.5, f = 0.2, n_\sigma = 1, \tau_a = \sigma_a, \tau_m = \sigma_m = 0, \delta = 0$. The ratio $\sigma_c/\tau_c$ equals: (a) $1/\sqrt{3}$; (b) $\sqrt{3}$.

diagram provides the accumulated damage measure on this plane. It is seen that damage occurs on different portions of the stress cycle and $\omega_{n\sigma}$ attains different values. Figures 8(a, b) provides similar diagrams for the combined in-phase loading by the bending and torsional moments, $\sigma_m = \tau_m = 0$, $\sigma_a = \tau_a$, $\delta = 0$, and for two strength ratios of $\sigma_c/\tau_c = 1/\sqrt{3}$ and $\sigma_c/\tau_c = \sqrt{3}$. Similarly as previously, damage accumulation for $\sigma_c/\tau_c = \sqrt{3}$ is considerably higher than that for $\sigma_c/\tau_c = 1/\sqrt{3}$. Figure 9(a, b) presents the damage accumulation diagrams for the out-of-phase combined loading, $\sigma_m = \tau_m = 0$, $\sigma_a = \tau_a$, $\delta = \pi/2$, and for two values of $\sigma_c/\tau_c$, as in previous diagrams.

Figures 10–12 present rosette diagrams of damage parameter distribution on physical planes inclined at the angle $\vartheta$ to the plane normal to cylinder axis. The damage evolution [given by relations (28) and (35)] was calculated for one loading cycle with account for the effect of phase angle $\delta$. In particular, Fig. 10(a, b) presents the rosette diagrams for $\sigma_c/\tau_c = 1/\sqrt{3}$ and $\sigma_c/\tau_c = \sqrt{3}$, in the case of pure bending loading, $\tau_m = \tau_a = 0$, and for three values of mean and amplitude stresses, $m = \sigma_m/\sigma_a$. It is seen that the maximal damage plane orientation essentially affected the values of $m$. Figure 11(a, b) presents the damage distribution for combined proportional loading and Fig. 12(a,b) corresponds to non-proportional loading.

Figure 13(a, b) provides the variation of fatigue damage accumulation factor $R_d$ with respect to the phase angle $\delta$ between normal and shear stresses in the cylinder cross-section for two damage evolution rules. The first rule is specified by eqns (28) and (31), the other by eqns (28), (34) and (35). It is seen that the first rule predict the decrease of damage accumulation for increasing values of phase angle. On the other hand, the second rule predicts both decrease and increase of $R_d$ depending on the value of strength parameter $\eta = \sqrt{3}\sigma_c/\tau_c$. For high strength steels for which $\sigma_c/\tau_c = 1.7$ the effect of the phase angle $\delta$ may be insignificant. This prediction is supported by some experiments [cf Zenner *et al.* (1985); Froustey and Lasserre (1989); McDiarmid (1991)]. Figure 14(a–c) presents the variation of $R_d$ against the phase angle for the second evolution rule eqns (28) and (35) and for different values of parameters: $\max(R_{f\sigma}) = 0.5$ and 0.4, $f = 0.2$ and 0.1, and $n_\sigma = 1.0$ and 2.0. These diagrams illustrate the model sensitivity with respect to parameter values.

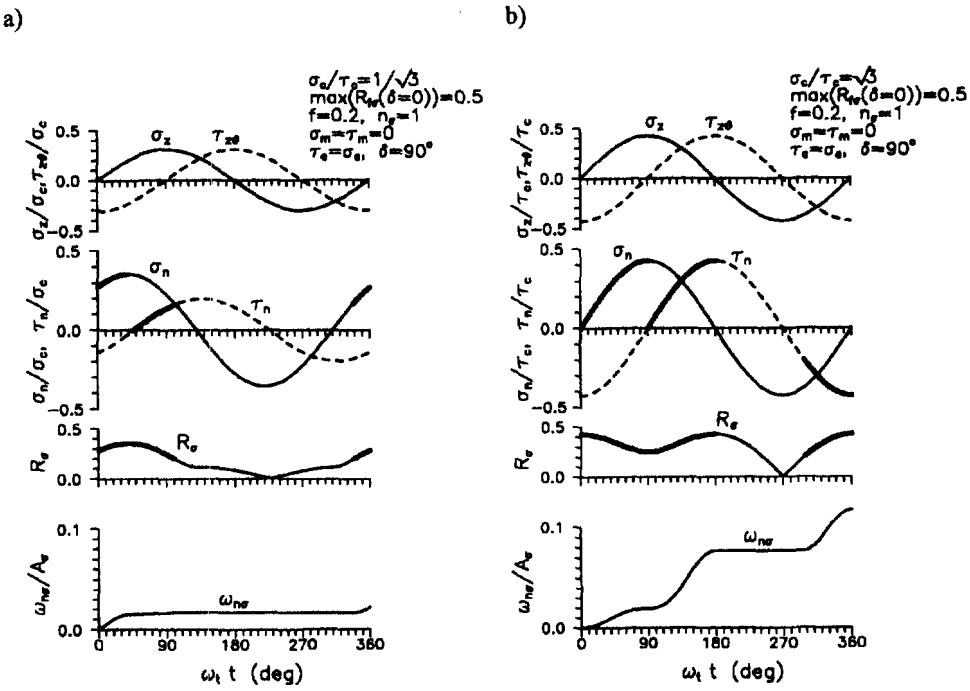


Fig. 9. Damage accumulation on the extremal plane during non-proportional bending and torsional one loading cycle for $\max(R_{f\sigma}) = 0.5, f = 0.2, n_\sigma = 1, \tau_m = \sigma_m = 0, \tau_a = \sigma_a, \delta = \pi/2$. The ratio $\sigma_c/\tau_c$ equals: (a) $1/\sqrt{3}$; (b) $\sqrt{3}$.

## 5. DAMAGE TENSOR AND COMPLIANCE VARIATION

The scalar damage distribution on physical planes predicted by the present model can be used in order to construct the tensor measure of damage. In fact, the function $\omega_n(\mathbf{n})$ can be generated for any loading program. The mean value of damage within the element is then obtained by integrating $\omega_n$ over all directions spanning the entire solid angle $\Omega = 4\pi$

$$\omega_0 = \frac{1}{4\pi}\int_{4\pi} \omega_n(\mathbf{n})\, d\Omega \tag{50}$$

and the maximal value

$$\omega_d = \max_{(\mathbf{n})} \omega_n(\mathbf{n}) \tag{51}$$

is used to specify the crack initiation condition. Following the previous work by Kanatani (1984), Onat and Leckie (1988), and Lubarda ad Krajcinovic (1993), we can consider the representation of damage by the second- and fourth-order tensors.

When the second-order damage tensor $\omega_{ij}$ is used, the damage measure on the physical plane equals

$$\omega(\mathbf{n}) = \omega_{ij} n_i n_j. \tag{52}$$

Considering a tensor $\omega_{ij}^*$ obtained from a known distribution $\omega_n(\mathbf{n})$, namely

$$\omega_{ij}^* = \frac{3}{4\pi}\int_{4\pi} \omega_n(\mathbf{n}) n_i n_j\, d\Omega. \tag{53}$$

It is easy to show that the tensors $\omega_{ij}$ and $\omega_{ij}^*$ are interrelated by the equation [cf Lubarda and Krajcinovic (1993)]

a)

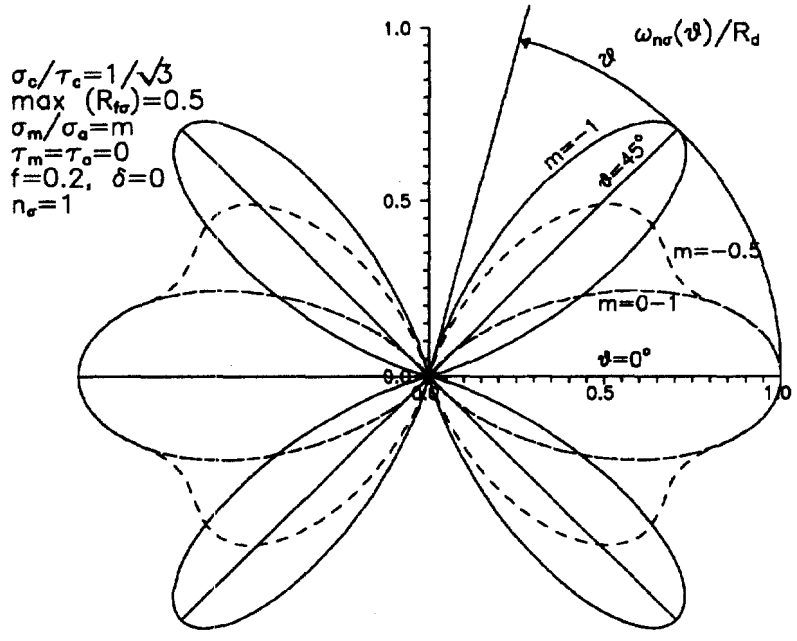


b)

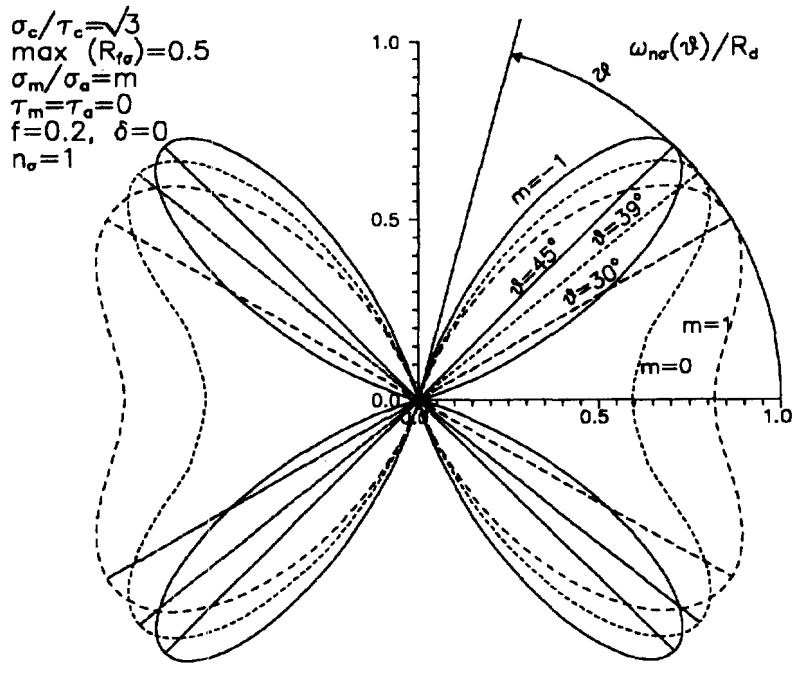


Fig. 10. Polar diagram of damage distribution $\omega_{n\sigma}(\vartheta)$ on material planes for bending loading: $\max(R_{f\sigma}) = 0.5$, $f = 0.2$, $n_\sigma = 1$, $\tau_a = \tau_m = 0$, $\sigma_m/\sigma_a = m$, $\delta = 0$ and for (a) $\sigma_c/\tau_c = 1/\sqrt{3}$; (b) $\sigma_c/\tau_c = \sqrt{3}$.

$$\omega_{ij} = \tfrac{5}{2}\omega_{ij}^* - \tfrac{3}{2}\delta_{ij}\omega_0. \tag{54}$$

Hence, the damage tensor $\omega_{ij}$ can be identified in terms of $\omega_{ij}^*$ and $\omega_0$ obtained from the known distribution of scalar damage on physical planes.

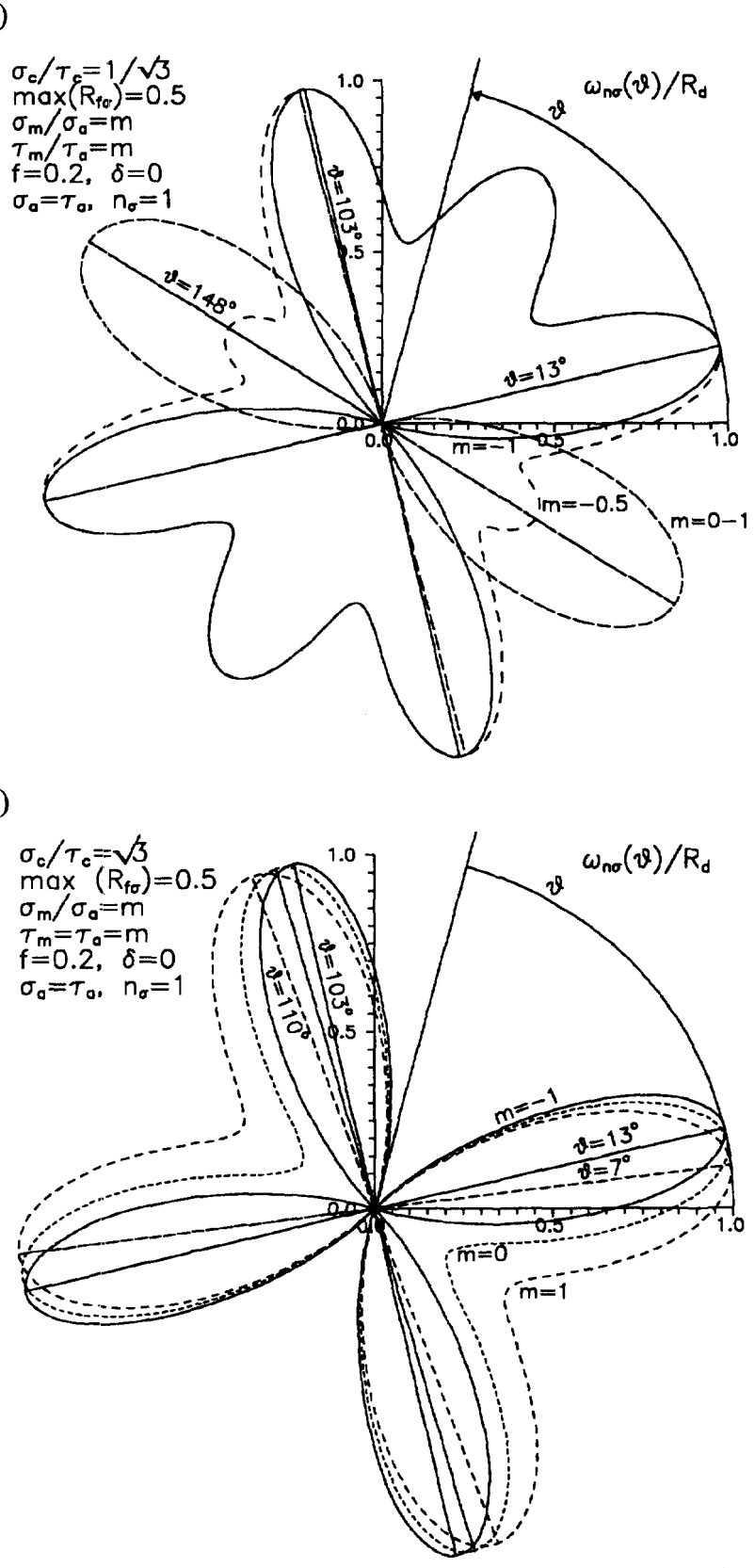


Fig. 11. Polar diagram of damage distribution $\omega_{n\sigma}(\vartheta)$ on material planes for proportional bending and torsional loading: $\max(R_{f\sigma}) = 0.5$, $f = 0.2$, $n_\sigma = 1$, $\tau_a = \sigma_a$, $\sigma_m/\sigma_a = m$, $\tau_m/\tau_a = m$, $\delta = 0$ and for $\sigma_c/\tau_c = 1/\sqrt{3}$; (b) $\sigma_c/\tau_c = \sqrt{3}$.

a)

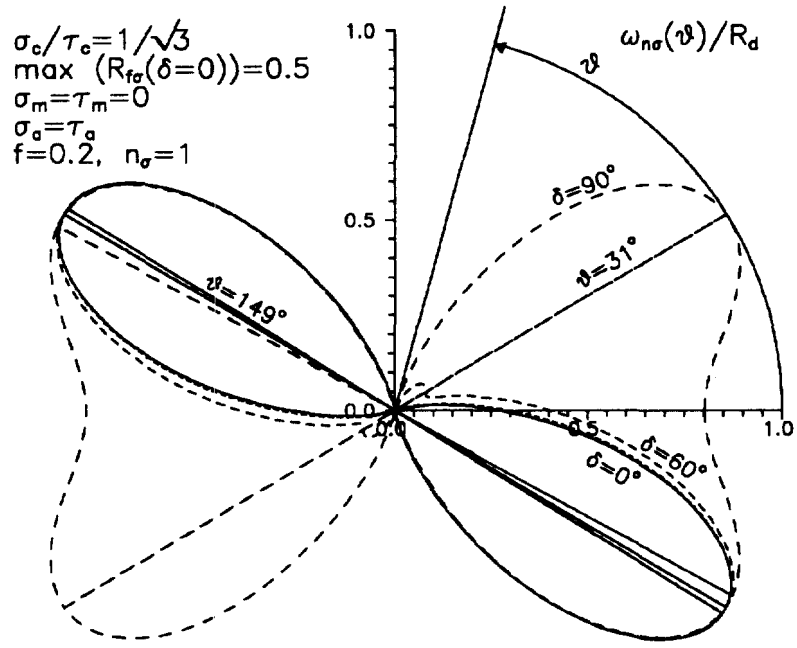


b)

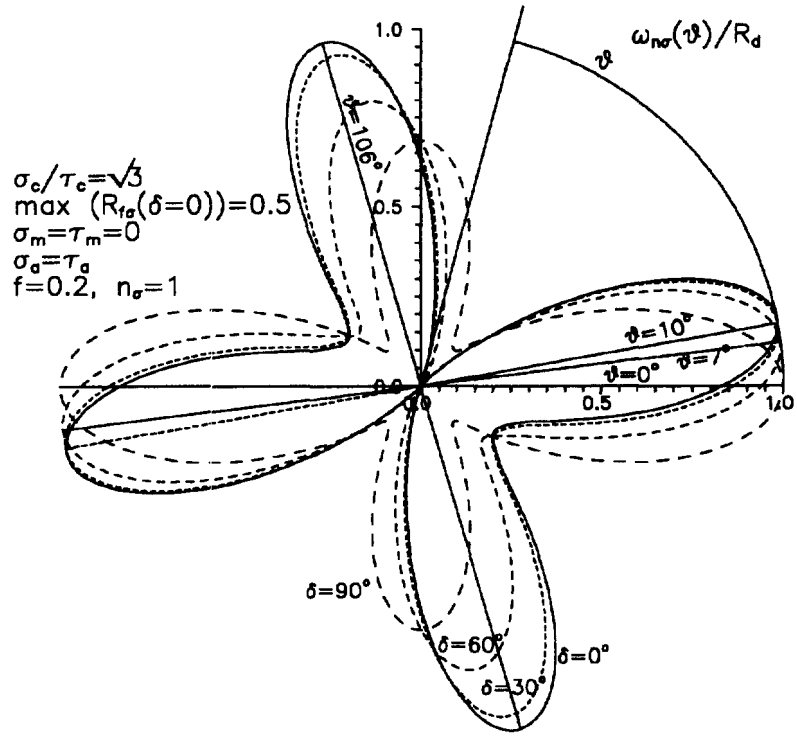


Fig. 12. Polar diagram of damage distribution $\omega_{n\sigma}(\vartheta)$ on material planes for non-proportional bending and torsional loading: $\max(R_{f\sigma}(\delta = 0)) = 0.5$, $f = 0.2$, $n_\sigma = 1$, $\tau_a = \sigma_a$, $\sigma_m = \tau_m = 0$, and for $\sigma_c/\tau_c = 1/\sqrt{3}$; (b) $\sigma_c/\tau_c = \sqrt{3}$.

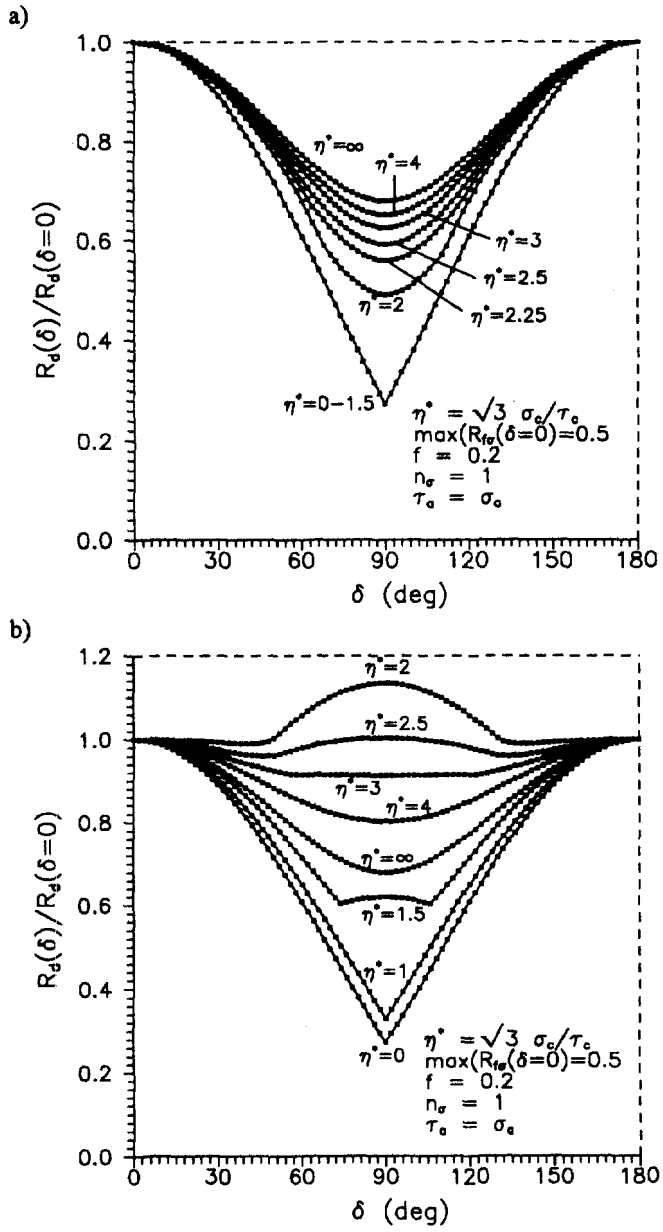


Fig. 13. Dependence of the fatigue damage accumulation factor $R_d$ on phase $\delta$ for bending and torsional loading: $\max(R_{f\sigma}(\delta = 0)) = 0.5, f = 0.2, n_\sigma = 1, \tau_a = \sigma_a, \sigma_m = \tau_m = 0$. (a) for the evolution rule (28), (31); (b) for the evolution rule (28), (35).

When the fourth-order damage tensor $\omega_{ijkl}$ is used, the damage measure on the physical plane is

$$\omega(\mathbf{n}) = \omega_{ijkl} n_i n_j n_k n_l. \tag{55}$$

On the other hand, knowing $\omega_n(n)$, the auxiliary damage tensor $\omega^*_{ijkl}$ can be generated, namely

$$\omega^*_{ijkl} = \frac{5}{4\pi} \int_{4\pi} \omega_n(\mathbf{n}) n_i n_j n_k n_l \, d\Omega. \tag{56}$$

The tensors $\omega_{ijkl}$ and $\omega^*_{ijkl}$ are now interrelated by the following equation

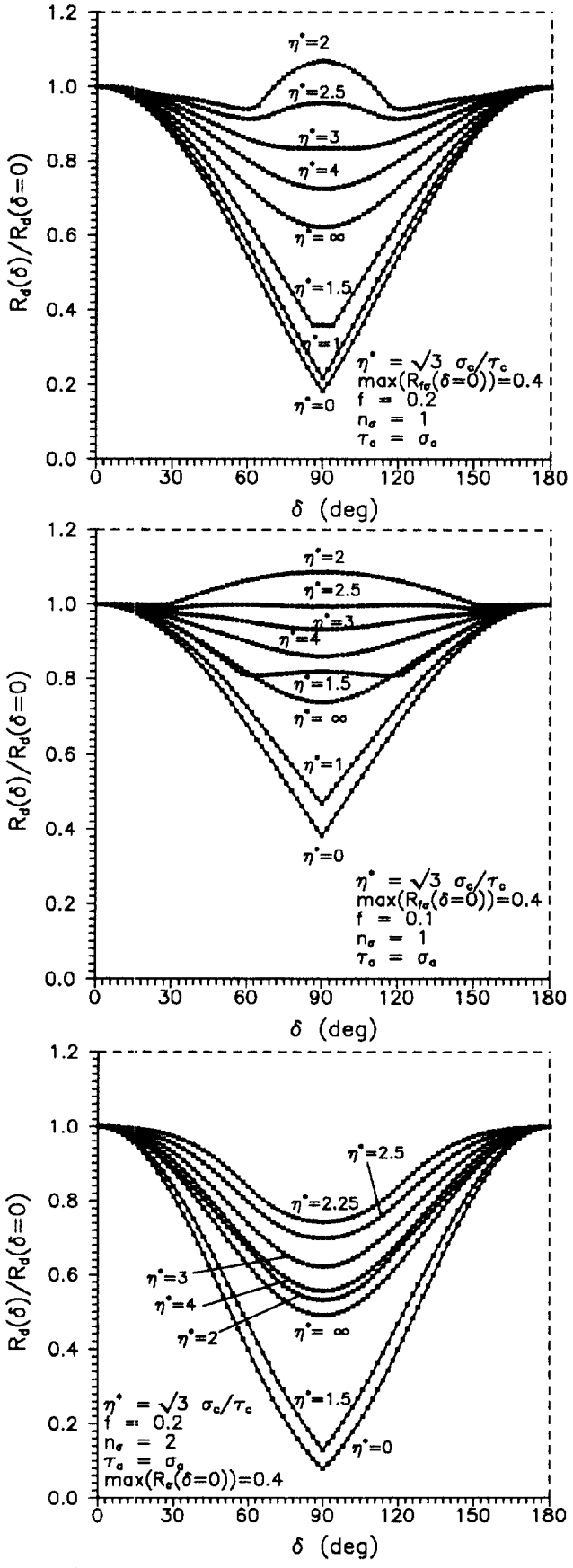


Fig. 14. Dependence of the fatigue damage accumulation factor $R_d$ on phase $\delta$ for the evolution rule (28), (35) and for: (a) $\max(R_{f\sigma}(\delta = 0)) = 0.4$, $f = 0.2$, $n_\sigma = 1$, $\tau_a = \sigma_a$, $\sigma_m = \tau_m = 0$; (b) $\max(R_{f\sigma}(\delta = 0)) = 0.4$, $f = 0.1$, $n_\sigma = 1$, $\tau_a = \sigma_a$, $\sigma_m = \tau_m = 0$; (c) $\max(R_{f\sigma}(\delta = 0)) = 0.4$, $f = 0.2$, $n_\sigma = 2$, $\tau_a = \sigma_a$, $\sigma_m = \tau_m = 0$.

$$\omega_{ijkl} = \tfrac{63}{8}\omega^*_{ijkl} - \tfrac{35}{4}A^*_{ijkl} + \tfrac{15}{8}\omega_0 I_{ijkl} \tag{57}$$

where

$$A^*_{ijkl} = \tfrac{1}{6}(\delta_{ij}\omega^*_{kl} + \delta_{kl}\omega^*_{ij} + \delta_{ik}\omega^*_{jl} + \delta_{il}\omega^*_{jk} + \delta_{jk}\omega^*_{il} + \delta_{jl}\omega^*_{ik})$$
$$I_{ijkl} = \tfrac{1}{3}(\delta_{ij}\delta_{kl} + \delta_{ik}\delta_{jl} + \delta_{il}\delta_{jk}). \tag{58}$$

Equation (57) provides the damage tensor $\omega_{ijkl}$ in terms of the specified distribution $\omega_n(\mathbf{n})$.

For the plane case, the respective formulae for $\omega_0$, $\omega^*_{ij}$ and $\omega^*_{ijkl}$ are

$$\omega_0 = \frac{1}{2\pi}\int_{2\pi} \omega_n(\vartheta)\,\mathrm{d}\vartheta$$
$$\omega^*_{ij} = \frac{1}{\pi}\int_{2\pi} \omega_n(\vartheta) n_i n_j\,\mathrm{d}\vartheta$$
$$\omega^*_{ijkl} = \frac{4}{3\pi}\int_{2\pi} \omega_n(\vartheta) n_i n_j n_k n_l\,\mathrm{d}\vartheta \tag{59}$$

and the damage tensor $\omega_{ij}$ and $\omega_{ijkl}$ are expressed as follows

$$\omega_{ij} = 2\omega^*_{ij} - \delta_{ij}\omega_0$$
$$\omega_{ijkl} = 6\omega^*_{ijkl} - 6A^*_{ijkl} + \omega_0 I_{ijkl}. \tag{60}$$

Figures 15 and 16 present the polar diagrams representing damage distribution on physical plane inclined at angle $\vartheta$ to the plane normal to the axis of a cylindrical specimen loaded by torsional and bending moments (the case discussed in the previous section). The damage distribution predicted by the damage stress condition (27)–(37) was approximated by the second- and fourth-order tensors. It is seen that the second-order damage tensor cannot describe adequately the damage distribution on physical planes. The accuracy of approximation depends on the number of extremal planes of damage. When two extremal planes occur, the fourth-order tensor should be used. Moreover, the negative values of damage are then predicted for some orientations (anticracks), similar to that which was observed by Lubarda and Krajcinovic (1993).

Consider now the elastic compliance variation due to damage evolution. Denoting by $C_{ijkl}$ the elastic compliance (or secant) matrix, we can write the rate (or incremental) equations

$$\dot{\varepsilon}_{ij} = C_{ijkl}\dot{\sigma}_{kl} + \dot{C}_{ijkl}\sigma_{kl} \tag{61}$$

where dot denotes the rate with respect to the evolution parameter or increment. The second term represents the damage strain rate due to variation of the compliance matrix. Denoting by $C^{\mathrm{e}}_{ijkl}$ the initial compliance matrix of te undamaged material, we have

$$C_{ijkl} = C^{\mathrm{e}}_{ijkl} + C^{\mathrm{d}}_{ijkl}$$
$$\varepsilon_{ij} = \varepsilon^{\mathrm{e}}_{ij} + \varepsilon^{\mathrm{d}}_{ij} = (C^{\mathrm{e}}_{ijkl} + C^{\mathrm{d}}_{ijkl})\sigma_{kl} \tag{62}$$

where $C^{\mathrm{d}}_{ijkl}$ represents the compliance growth due to accumulated damage.

Assume now that the damage strain is developed on each physical plane depending on the damage state (Fig. 17). We can write, therefore,

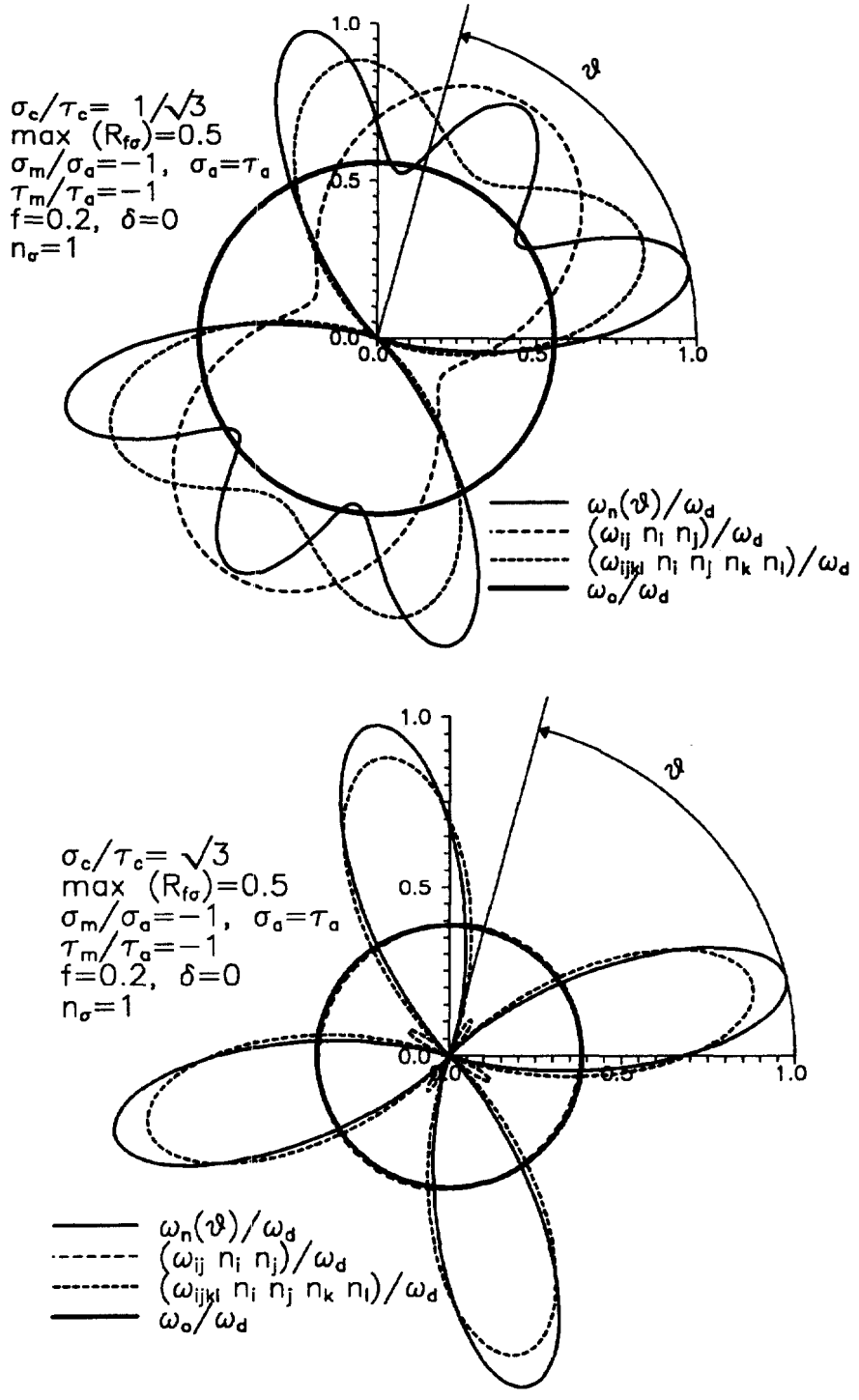


Fig. 15. Rosette diagrams of damage distribution $\omega_n(\vartheta)$ and their approximations by the second and fourth order damage tensors for proportional bending and torsional loading: $\max(R_{f\sigma}) = 0.5$, $f = 0.2$, $n_\sigma = 1$, $\delta = 0$, $\tau_a = \sigma_a$, $\sigma_m/\sigma_a = \tau_m/\tau_a = -1$. The ratio $\sigma_c/\tau_c$ equals: (a) $1/\sqrt{3}$; (b) $\sqrt{3}$.

$$\varepsilon_n^d = \varepsilon_n^d(\sigma_n, \omega_n) \quad \gamma_n^d = \gamma_n^d(\tau_n, \omega_n). \tag{63}$$

In what follows we shall consider only normal damage strain component, depending linearly on normal stress and on the damage parameter, thus

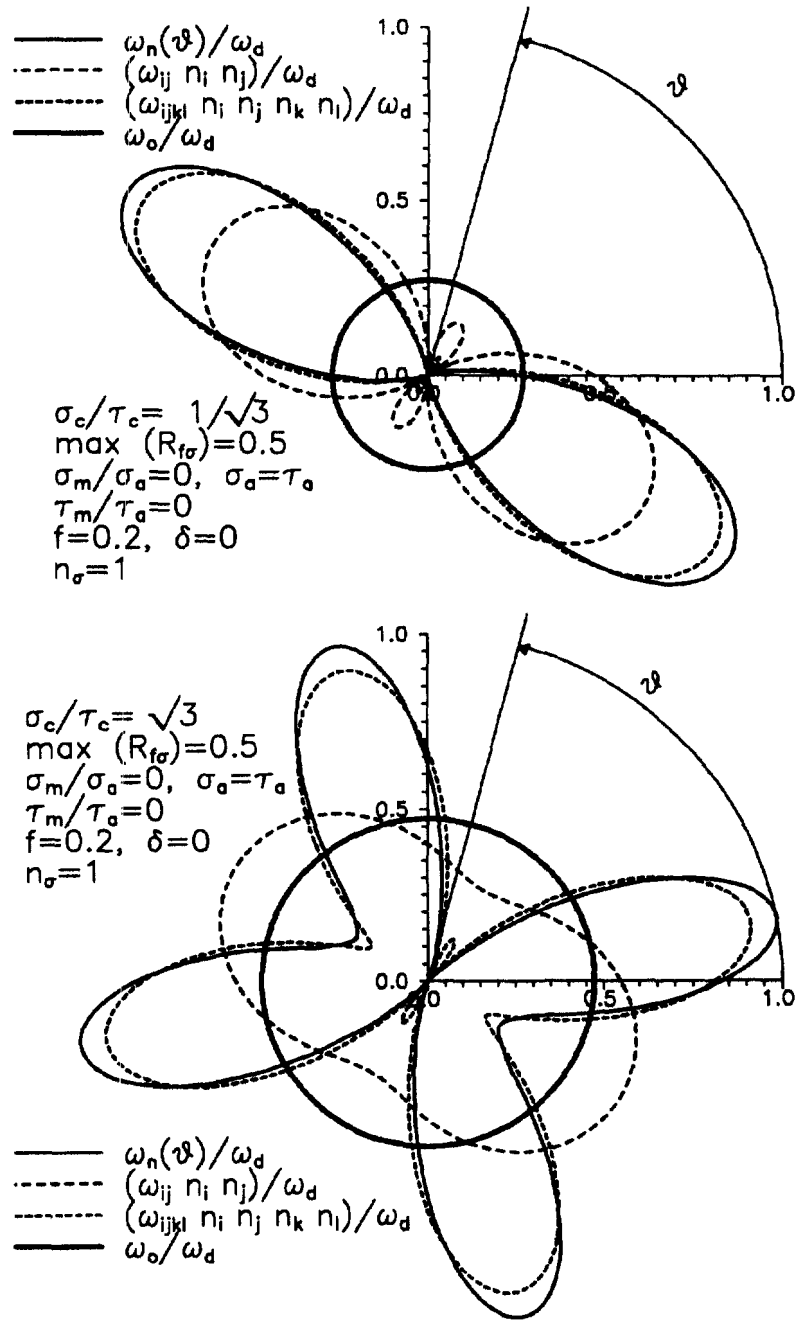


Fig. 16. Rosette diagrams of damage distribution $\omega_n(\vartheta)$ and their approximations by the second and fourth order damage tensors for proportional bending and torsional loading: $\max(R_{f\sigma}) = 0.5$, $f = 0.2$, $n_\sigma = 1$, $\delta = 0$, $\tau_a = \sigma_a$, $\sigma_m = \tau_m = 0$. The ratio $\sigma_c/\tau_c$ equals: $1/\sqrt{3}$; (b) $\sqrt{3}$.

$$\varepsilon_n^d = A_n \left(\frac{\omega_n}{1-\omega_n}\right)^q \langle\sigma_n\rangle = C_n^d \sigma_n \tag{64}$$

where $A_n$ and $q$ are material parameters, and $\langle\sigma_n\rangle = \sigma_n$ for $\sigma_n \geqslant 0$, $\langle\sigma_n\rangle = 0$ for $\sigma_n < 0$. The normal damage compliance now equals

$$C_n^d = A_n \left(\frac{\omega_n}{1-\omega_n}\right)^q H(\sigma_n) \tag{65}$$

where $H(\sigma_n)$ is the Heaviside function, $H(\sigma_n) = \langle\sigma_n\rangle/\sigma_n$. Following the derivations of the damage tensor, let us calculate the auxiliary compliance tensors

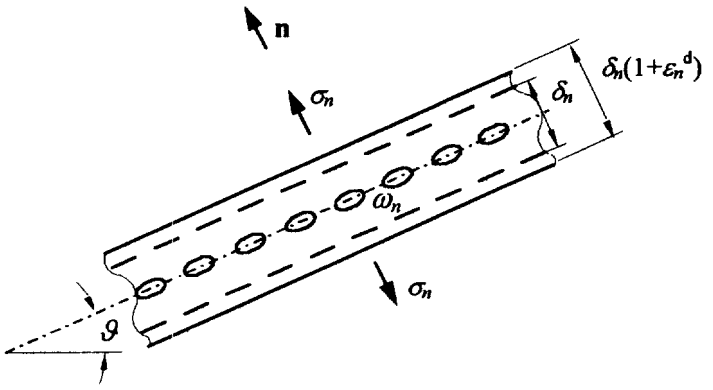


Fig. 17. Strain increase induced by accumulated damage on the physical plane.

$$C_0^{d*} = \int_{4\pi} C_n^d(\mathbf{n})\,d\Omega$$

$$C_{ij}^{d*} = \int_{4\pi} C_n^d(\mathbf{n}) n_i n_j\,d\Omega$$

$$C_{ijkl}^{d*} = \int_{4\pi} C_n^d(\mathbf{n}) n_i n_j n_k n_l\,d\Omega. \tag{66}$$

The compliance tensor due to accumulated damage is now expressed as follows:

$$C_{ijkl}^d = \frac{315}{32\pi}\left(C_{ijkl}^{d*} - \frac{2}{3}A_{ijkl} + \frac{C_0^{d*}}{21}I_{ijkl}\right) \tag{67}$$

where

$$A_{ijkl} = \tfrac{1}{6}(\delta_{ij}C_{kl}^{d*} + \delta_{kl}C_{ij}^{d*} + \delta_{ik}C_{jl}^{d*} + \delta_{il}C_{jk}^{d*} + \delta_{jk}C_{il}^{d*} + \delta_{jl}C_{ik}^{d*})$$
$$I_{ijkl} = \tfrac{1}{3}(\delta_{ij}\delta_{kl} + \delta_{ik}\delta_{jl} + \delta_{il}\delta_{jk}). \tag{68}$$

For the plane case, we obtain

$$C_0^{d*} = \int_{2\pi} C_n^d(\vartheta)\,d\vartheta$$

$$C_{ij}^{d*} = \int_{2\pi} C_n^d(\vartheta) n_i n_j\,d\vartheta$$

$$C_{ijkl}^{d*} = \int_{2\pi} C_n^d(\vartheta) n_i n_j n_k n_l\,d\vartheta \tag{69}$$

and

$$C_{ijkl}^d = \frac{8}{\pi}C_{ijkl}^{d*} - \frac{6}{\pi}A_{ijkl} + \frac{C_0^{d*}}{2\pi}I_{ijkl}. \tag{70}$$

Let us apply the present formulae to the case of uniaxial tension. Assuming the failure stress function $R_\sigma$ in the form (4), the follows eqns (12) and (34), the increment of $R_\sigma$ is expressed as follows:

$$d\hat{R}_\sigma = \frac{\langle d\sigma_n \rangle}{\sigma_{c0}(1-\omega_{n\sigma})^p} + \frac{p\langle \sigma_n \rangle d\omega_{n\sigma}}{\sigma_{c0}(1-\omega_{n\sigma})^{p+1}}. \tag{71}$$

Further, it is assumed that $\sigma_0/\sigma_c = f = \text{const}$. The damage growth is specified by the relation

$$d\omega_n = \frac{\Psi_\sigma \langle d\sigma_n \rangle}{\sigma_c \left(1 - \Psi_\sigma \dfrac{p\langle \sigma_n \rangle}{\sigma_c(1-\omega_{n\sigma})}\right)} \tag{72}$$

where

$$\Psi_\sigma = A_\sigma \left(\frac{\sigma_n + \sigma_0}{\sigma_c(1-f)}\right)^{n_\sigma} \frac{1}{1-f}. \tag{73}$$

The stress–strain relation can now be obtained in the form

$$\sigma = \frac{\varepsilon E_0}{1 + A_n E_0 \left(\dfrac{\omega_n}{1-\omega_n}\right)^q H(\sigma)} \tag{74}$$

where $E_0$ denotes the initial value of Young modulus.

Figure 18(a–c) presents the stress–strain relations, evolution of damage $\omega_{n\sigma}$, and variation of failure stress $\sigma_c$ on the plane normal to the tension direction. It is seen that for different values of parameters $A_n E_0$, $q$ and $p$ the deformation response may differ significantly. In Fig. 18(c) the stable portion of stress–strain curve is followed by a softening portion associated with the growing damage. A more detailed study of compliance variation of damaged materials will be provided in a separate paper.

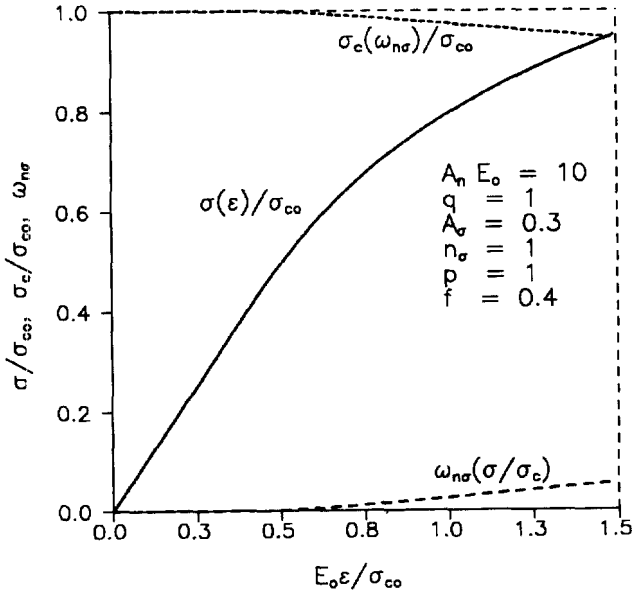


Fig. 18. Stress–strain relations, evolution of damage and of failure stress for different values of compliance variation parameters: (a) $f = 0.4$, $p = 1$, $q = 1$, $A_\sigma = 0.3$, $n_\sigma = 1$, $A_n E_0 = 10$; (b) $f = 0.4$, $p = 1$, $q = 1$, $A_\sigma = 0.4$, $n_\sigma = 1$, $A_n E_0 = 20$; (c) $f = 0.2$, $p = 2.5$, $q = 2$, $A_\sigma = 0.6$, $n_\sigma = 1$, $A_n E_0 = 50$.

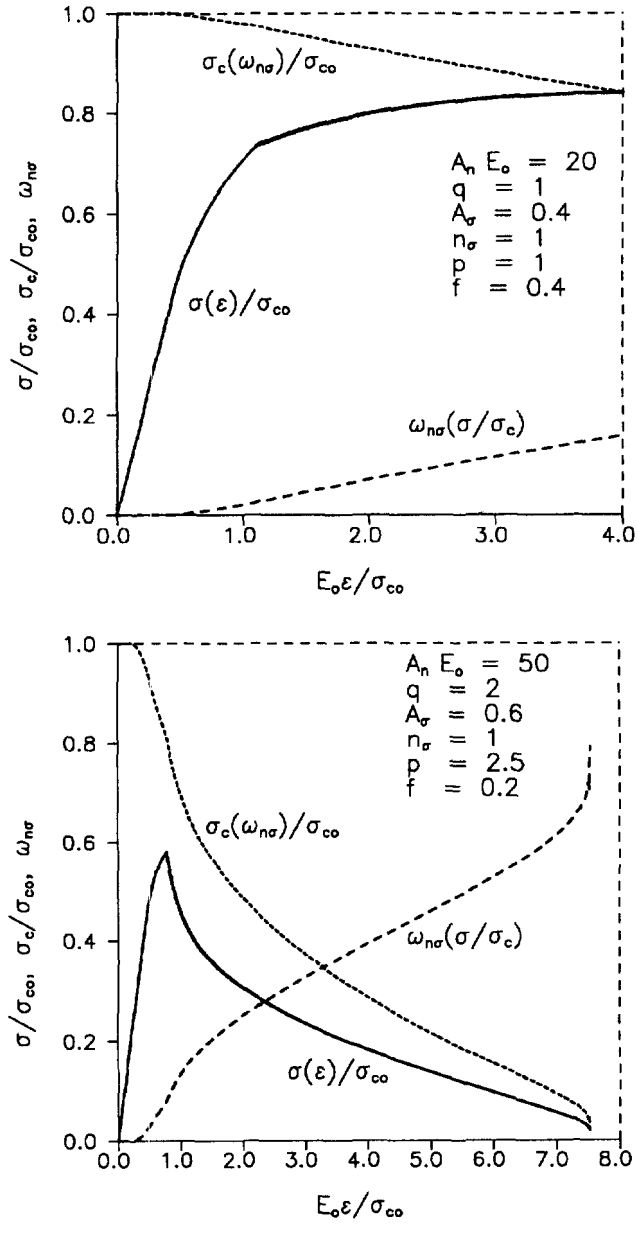


Fig. 18—*Continued.*

## 6. CONCLUDING REMARKS

In this paper, the damage and fracture conditions were expressed in terms of interface stresses or strains. The damage distribution within the element can then be determined and the crack initiation is assumed to occur within the plane of maximal damage. For high cycle fatigue loading or for some brittle materials under static loading the variation of compliance preceding crack initiation can be neglected.

The analysis can then be carried out within the linear elasticity model. On the other hand, the effect of accumulated damage on strength parameters can be accounted for. The singular and regular stress regimes can be uniformly treated by applying the non-local condition. Thus, the crack initiation can be predicted or any defect or inhomogeneity generating stress concentration.

The present paper provides also an alternative way to describe the damage distribution within the macroscopic element. Instead of formulating tensor damage variables and dependence of free energy function on these variables, the damage distribution function $\omega_n(\mathbf{n})$ is

obtained from the relevant interfacial damage condition. The compliance variation and the free energy function can next be determined from the specified damage distribution. This way seems much simpler and is naturally related to experimental identification of microcracking in brittle materials.

## REFERENCES


Budiansky, B. and O'Connell, R. J. (1976) Elastic moduli of a cracked solid. *International Journal of Solids and Structures* **12,** 81–97.

Chaboche, J. L. (1992) Damage induced anisotropy: on the difficulties associated with the active/passive unilateral condition. *International Journal of Damage Mechanics* **1,** 148–171.

Dragon, A. and Mróz, Z. (1979) A continuum model for plastic–brittle behavior of rock and concrete. *International Journal of Engineering Science* **17,** 121–137.

Froustey, C. and Lasserre, S. (1989) Multiaxial fatigue endurance of 30NCD16 steel. *International Journal of Fatigue* **11,** 169–175.

Griffith, A. A. (1920) The phenomena of rupture and flowing solids. *Philosophical Transactions of the Royal Society A* **221,** 163–198.

Horii, H. and Nemat-Nasser, S. (1983) Overall moduli of solids with microcracks: load-induced anisotropy. *Journal of Mechanics and Physics of Solids* **31,** 155–171.

Hussain, M. A., Pu, S. L. and Underwood, J. (1974) Strain energy release rate for a crack under combined Mode-I and -II. *ASTM STP* **560,** 2–28.

Irwin, G. (1957) Analysis of stresses and strains near the end of crack traversing a plate. *Journal of Applied Mechanics* **24,** 361–365.

Kachanov, L. M. (1958) On the creep rupture time. *Izv. A. N. SSSR, Otd. Techn. Nauk* **8,** 26–31 (in Russian).

Kanatani, K. (1984) Distribution of directional data and fabric tensors. *International Journal of Engineering Science* **22,** 149–164.

Krajcinovic, D. (1989) Damage mechanics. *Mechanics of Materials* **8,** 117–197.

Lemaitre, J. (1992) *A Course on Damage Mechanics*. Springer, Berlin.

Lubarda, V. A. and Krajcinovic, D. (1993) Damage tensors and the crack density distribution. *International Journal of Solids and Structures* **30,** 2859–2877.

Lubarda, V. A. and Krajcinovic, D. (1994) Tensorial representation of the effective elastic properties of the damaged materials. *International Journal of Damage Mechanics* **3,** 38–56.

McDiarmid, D. L. (1991) A general criterion for high-cycle multiaxial fatigue failure. *Fatigue and Fracture Engineering Materials and Structures* **14,** 429–453.

Mróz, Z. (1983) Hardening and degradation rules for metals under monotonic and cyclic loading. *Journal of Engineering Material Technology, Transactions of the ASME* **105,** 113–119.

Murakami, S. (1988) Mechanical modelling of material damage. *Journal of Applied Mechanics* **55,** 280–286.

Novozhilov, V. V. (1969) On necessary and sufficient criterion of brittle fracture. *Prikl. Mat. Mekh (PMM)* **33,** 212–216 (in Russian).

Onat, E. T. and Leckie, F. A. (1988) Representation of mechanical behavior in the presence of changing internal structure. *Journal of Applied Mechanics* **55,** 1–10.

Palaniswamy, K. and Knauss, E. G. (1972) Propagation of a crack under general in-plane tension. *International Journal of Fracture Mechanics* **8,** 114–117.

Seweryn, A. (1994) Brittle fracture criterion for structures with sharp notches. *Engineering Fracture Mechanics* **47,** 673–681.

Seweryn, A. and Mróz, Z. (1994) A non-local mixed mode fracture initiation and propagation condition for monotonic and cyclic loading. In *Proceedings of the Fourth International Conference on Biaxial/Multiaxial Fatigue*, St Germain en Laye, Vol. 1, pp. 499–512.

Seweryn, A. and Mróz, Z. (1995) A non-local stress failure condition for structural elements under multiaxial loading. *Engineering Fracture Mechanics* **51,** 955–973.

Seweryn, A. and Mróz, Z. (1996) A non-local stress failure and fatigue damage accumulation condition. In *Multiaxial Fatigue and Design* eds A. Pineau, G. Cailletaud and T. Lindley. Mechanical Engineering Publications, London, pp. 259–280.

Seweryn, A., Poskrobko, S. and Mróz, Z. (1997) Brittle fracture in plane elements with sharp notches under mixed-mode loading. *Journal of Engineering Mechanics ASCE* **123** (in print).

Sih, G. C. (1974) Strain-energy-density factor applied to mixed mode crack problems. *International Journal of Fracture* **10,** 305–321.

Simo, J. C. and Ju, J. W. (1987) Strain and stress based continuum damage models—I Formulation. *International Journal of Solids and Structures* **23,** 821–840.

Wells, A. A. (1961) Critical tip opening displacement as fracture criterion. In *Proceedings of the Crack Propagation Symposium*, Cranfield, Vol. 1, pp. 210–221.

Zenner, H., Heidenreich, R. and Richter, I. (1985) Dauerschwingfestigkeit bei nichtsynchroner mehrachsiger Beanspruchung. *Zeitschrift Werkstofftech* **16,** 101–112.